Journal of Energy Storage 73 (2023) 108819

Contents lists available at ScienceDirect

Journal of Energy Storage

journal homepage: www.elsevier.com/locate/est

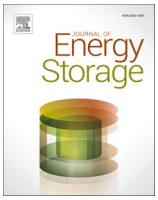

Research Papers

A novel experimental method of power smoothing using supercapacitors and hydrogen for hybrid system PV/HKT

Paul Arévalo [a,b], Antonio Cano [a], Francisco Jurado [a,*]

[a] Department of Electrical Engineering, University of Jaen, 23700 EPS Linares, Jaen, Spain
[b] Department of Electrical, Electronics and Telecommunications Engineering (DEET), University of Cuenca, Cuenca 010107, Ecuador

ARTICLE INFO

Keywords:
Hydrogen
Experimental test
Hydrokinetic turbine
Photovoltaic
Power smoothing

ABSTRACT

Nowadays, the intermittent nature of renewable energy systems represents one of the most significant challenges in isolated systems, where power fluctuations can cause instability and compromise energy quality. Although hydrogen systems and supercapacitors have been widely studied in the literature, they have been less investigated as participating agents, and further research is needed in this area. This paper presents a novel power smoothing method for an off-grid system that consist of photovoltaic panels, hydrokinetic turbines, fuel cells and a hybrid storage system (hydrogen and supercapacitors). Two well-known power smoothing methods were used to generate the power signals for the new method. The main novelty is based on controlling the state of charge of the supercapacitor using the fuel cell, for the reduction of power fluctuations and efficiently hydrogen produce. First, the capacity of the renewable system is optimized using the HOMER Pro software. Then, the optimized system was used to simulate the new method proposed in Matlab-Simulink. Finally, to validate the results obtained, extensive experiments were conducted in a laboratory test bench. The results showed that the power fluctuations index was reduced by up to 50 % in the electrolyzer and 20 % in the fuel cell, with a levelized cost of electricity of 0.19 USD/kWh. Therefore, the application of the new proposed energy smoothing method significantly improves hydrogen production.

1. Introduction

The adverse climate impact associated with fossil fuels has prompted changes in energy policy in several countries [1], with the electricity sector being a significant source of polluting gases [2]. The latter deserves to be carefully analyzed due to challenges in accessing remote areas [3]. One of the proposed solutions is the development of new environmentally-friendly technologies, including photovoltaic energy (PV), which is a promising alternative to provide electricity to remote off-grid locations [4]. Unfortunately, the intermittent nature of renewable energy sources (RES) gives rise to technical challenges due to factors like cloud movement, which compromises the stability of renewable systems [5]. Researchers have proposed various techniques to mitigate power fluctuations. For instance, some suggest using batteries to absorb power peaks caused by PV panels [6]. Energy storage systems play a vital role in maintaining the energy balance between supply and demand, particularly in isolated systems [7]. Lithium-ion and lead-acid batteries are commonly used for smoothing power fluctuations, but they require a well-designed control strategy to effectively regulate their state of charge (SOC) [8]. However, subjecting batteries to rapid and deep charge/discharge cycles may decrease their lifespan [9]. To address this issue, various researchers have proposed the use of hybrid energy storage systems (HESS) comprising both supercapacitors (SC) and batteries to smoothen power fluctuations. Wang et al. [10] propose a power smoothing technique for a grid-connected PV plant using SC to reduce power peaks and prevent batteries from operating at low SOC levels. The effectiveness of their approach is demonstrated through extensive computational simulations. The power smoothing methods explored in the literature aim to enhance the energy quality of grid-connected systems. According to Shivashankar et al. [11], the most commonly used HESS are batteries and SCs, with moving average being the prevalent power smoothing method in the literature. A groundbreaking technology that has revolutionized energy storage is green hydrogen (H_2) [12]. Compared to diesel generators, fuel cells are higher efficient, reliable, faster load tracking, and cleaner operation with fewer greenhouse gas emissions, making them ideal for off-grid installations. Moreover, the use of H_2 in power smoothing applications is relatively new. Valverde et al. [12] presents a laboratory study comparing the performance of various energy storage systems, indicating that fuel cells

* Corresponding author.
E-mail address: fjurado@ujaen.es (F. Jurado).

https://doi.org/10.1016/j.est.2023.108819
Received 5 May 2023; Received in revised form 22 July 2023; Accepted 22 August 2023
Available online 1 September 2023

Nomenclature

Acronyms

HOMER	Hybrid Optimization of Multiple Energy Resources
LCOE	Levelized cost of electricity
PV	Photovoltaic
SOC	State of charge
HESS	Hybrid energy storage system
SC	Supercapacitor
H_2	Hydrogen
Elz	Electrolyzer
FC	Fuel cell
DC	Direct current
AC	Alternating current
ELES	Enhanced Linear Exponential Smoothing
EMA	Exponential Moving Average
HKT	Hydrokinetic turbine
MPPT	Maximum power point tracking
HRES	Hybrid renewable energy system
HEC-RAS	Hydrologic Engineering Center - River Analysis System
INAMHI	National Institute of Meteorology and Hydrology
SCADA	Supervisory Control and Data Acquisition
CC	Cycle charging
CD	Combined dispatch
LF	Load following
NPC	Net present cost
FSR	Fluctuation suppression rate
MSOC	Mean state of charge

Sets

Ξ	Set of the several power smoothing methods
t	Index for time

Parameters and decisions variables

T	Number of time intervals
P_t^{PV}	PV output power
γ_t^{PV}	PV rated capacity
λ^{PV}	PV derating factor
$I_{T,t}^{PV}$	PV current generated
$I_{S,t}^{PV}$	Reverse saturation diode current
α_{pw}^{PV}	Power temperature coefficient
T_C^{PV}	Cell temperature
T_S^{PV}	Cell temperature under standard test conditions
P_t^{HKT}	HKT output power
P_t^{hkt}	HKT output power without boundary conditions
ξ_t	Index of maximum overpower value in HKT
ρ^{ω}	Water density
A^{HKT}	HKT sweep surface
α_t	River speed
ζ_p^{HKT}	HKT power coefficient
η^{HKT}	HKT efficiency
$\overline{P_t^{HKT}}$	Maximum HKT power allowed
E_t^{SC}	Energy stored in SC
C^{SC}	Capacitance of SC
V_t^{SC}	Nominal voltage in SC
SOC_t^{SC}	State of charge in SC
$SOC_{min,t}^{SC}$	Minimum state of charge in SC
$SOC_{max,t}^{SC}$	Maximum state of charge in SC
V_t^{min}	SC voltage lower limit
V_t^{max}	SC voltage upper limit
$I_t^{Ch,max}$	Maximum charge current allowed in SC
I_t^{SC}	Nominal current in SC
$I_t^{Dis,max}$	Maximum discharge current allowed in SC
U_t^{cell}	Fuel cell voltage
ΔG	Gibbs power exchange
ΓF	Transferred electrons, F is Faraday constant
r_i	Resistance value of the electrolyte $(i = 1, 2)$
T_{Elz}	Electrolyte temperature
A^{cell}	Fuel cell area
I_t^{Elz}	DC current drawn in electrolyzer
s_i and t_i	Overvoltage of the electrodes $(i = 1 \ldots 3)$
U^{Elz}	Elz cell voltage
N^{Elz}	Number of cells
$C^{int,Elz}$	Thermal capacitance of the Elz
$\dot{Q}_t^{fc\_gen}$	Internal heat
$\dot{Q}_t^{Elz\_loss}$	Heat losses
$\dot{Q}_t^{Elz\_cool}$	Cooling load for auxiliary services
ΔH	Enthalpy change
T_a	Ambient temperature
R^{t_Elz}	Elz total thermal resistance
T_{cwi}	Temperature of the inlet cooling water
h^{cond}	Heat transfer by conduction
h^{conv}	Heat transfer by convection
$\dot{\eta}_{H_2}$	Rate of hydrogen production
η_F	Faraday efficiency
a_i	Represent the efficiency of the Faraday ratio $(i = 1 \ldots 5)$
C^{cw}	Heat capacity of the cooling water
V_t^{FC}	Voltage at the FC terminals
N^{FC}	Number or FC cells
E_t^{nernst}	Equilibrium voltage
V_t^{act}	Activation voltage
V_t^{ohm}	Ohmic voltage
V_t^{con}	Concentration voltage
ΔS	Molar entropic variation in standard conditions
T_t^{ref}	Cell reference temperature
T_t^{FC}	Temperature of FC
R	Represent the constant of the gas
P_{H_2}	Hydrogen partial pressure
P_{O_2}	Effective partial pressure of oxygen
xi $(i = 1, \ldots, 4)$	Coefficients from the thermodynamic model
I_t^{FC}	Current of FC
C_{O_2}	Oxygen concentration
R^{ohm}	Algebraic sum of the resistances
R^m	Equivalent impedance
R^c	Contact resistance between the membrane and the electrodes
r^m	Resistivity of the membrane
l	Membrane thickness
A	Membrane activation area
β	Constant determined by the FC
ψ	Nominal current density
ψ_{max}	Maximum allowable current density
T_t^{an}	Temperature of the gas accumulation in the anode
V_t^{an}	Volume of the anode
$\dot{m}_{H_2}^{in}$	Hydrogen inlet mass flow rate
$\dot{m}_{H_2}^{react}$	Hydrogen reaction mass flow rate
$\dot{m}_{H_2}^{out}$	Outlet mass flow rate of hydrogen
T_t^{ca}	Gas temperature in cathode
V_t^{an}	Cathode control volume
$\dot{m}_{O_2}^{in}$	Oxygen inlet mass flow rate
$\dot{m}_{O_2}^{react}$	Reaction oxygen mass flow rate
$\dot{m}_{O_2}^{out}$	Oxygen output mass flow rate

C^{t_FC}	Thermal capacitance of the FC
$\dot{Q}^{FC\_gen}$	Heat generated by the chemical reaction of energy conversion
P^{FC}	Power output produced by FC
$\dot{Q}^{FC\_cool}$	Amount of energy for cooling
$\dot{Q}^{FC\_loss}$	Amount of energy for looses
N^{FC}	Number of cells connected in series within FC
V^{stack}	Voltage in FC terminals
T_t^{cwo}	Outlet cooling water temperature
R^{t_FC}	Overall thermal resistance of the FC
P_t^l	Electric demand power flow
$SOC_t^{H_2}$	State of charge in hydrogen tank
$SOC_{min,t}^{H_2}$	Minimum state of charge in hydrogen tank
$P_{ref,t}^{HRES}(k)$	Reference power signal
$P_t^{EMA}(k)$	Output power applying the EMA method
α	Represents the power smoothing coefficient in EMA method
P_t^{ELES}	Output power applying the ELES method
ϱ	Smoothing factor in ELES method
$P_t^{net,l}$	Net power
P_{ref}^{FC}	Power signal for FC
P_{ref}^{Elz}	Power signal for Elz
P_{ref}^{SC}	Power signal for SC
SP	Start point of the loop
FP	Finish point of the loop
M_{ti}	Fluctuation control mode (EMA or ELES) at instant i of the period of interest

possess high energy density, making them suitable for peak shaving applications. This capability allows surplus electricity produced by RES to be stored as H_2 using an electrolyzer (Elz) and subsequently generate electrical energy through a fuel cell (FC). While there are significant economic challenges to overcome, such as optimization the sizing of the H_2 tank, Elz and FC, several authors have demonstrated the feasibility of sizing optimization in a hybrid renewable energy system (HRES) using the HOMER Pro software. HOMER Pro is specifically designed for this purpose and is widely used in the literature [13–16]. Additionally, this software can simulate PV systems combined with SC [17]. Due to the stochastic behaviour of RES, data for at least one year will be necessary. HOMER Pro calculates the optimal size of components from an economic standpoint, reducing the unmet load.

In the literature, researchers have explored the use of H_2 to mitigate power fluctuations. Abdelghany et al. [18] propose a model and control system for H_2 to smooth power in a wind farm connected to the grid. However, they find that high fluctuations can negatively impact the lifespan of the H_2 tank, Elz and FC, resulting in reduced system performance. Kong et al. [19], a novel power smoothing method focused on optimizing the sizing of the Elz and FC for a renewable PV/Wind farm system is proposed. While the system effectively reduces power fluctuations, it faces some challenges with high ramp rates. Similarly, Takahashi et al. [20], a novel smoothing method for a grid-connected PV system is presented, focusing on H_2 production with an Elz. The results show that this configuration can reduce power fluctuations for intervals of $<$1000 s. However, the slow response of H_2 significantly limits its effectiveness in smoothing of power fluctuations.

Based on the studies presented in the literature review, it is evident that there are several drawbacks to overcome for H_2 systems to efficiently and rapidly smooth power peaks. For instance, the impact on the lifespan in FC and Elz, as well as the slow response of FC, are critical issues. Some solutions to these problems have been proposed, including the integration of SC in a HESS to better handle power fluctuations, as suggested in Kong et al. [21]. The authors combine SC/FC, reducing power peaks in a grid connected PV system, and computational results show that the fast response of SC improves FC behaviour. However, the operating limits of SC and FC have not been considered in their study. Nempu et al. [22], a method to reduce PV and wind power fluctuations using SC and FC is proposed. The novelty lies in the separation of two sub-grids (DC and AC) for the PV system and wind farm, respectively. SC and FC are employed for power smoothing in the PV sub-grid, while only SC is used for peak shaving in the wind farm sub-grid. The results suggest that the technique works effectively for both sub-grids, but the need to reset the two systems with different reference signals may increase computational efforts, and the reference signal remains strongly tied to the utility grid.

The studies mentioned above focus on HRES connected to utility grid, and there is limited research on H_2 systems to smooth power peaks in off-grid systems, making such applications uncommon. Tesfahunegn et al. [23], a power smoothing method is proposed for an off-grid PV system using a HESS composed of H_2 and lead-acid batteries. This configuration allows the batteries to operate in a high SOC band, avoiding deep discharges that reduce the lifespan of lead-acid batteries. While this approach has it benefits, it necessitates the development of new techniques and equipment combinations to enhance technical and economic efficiency in power smoothing methods for off-grids using H_2 as the main energy vector. The moving average is a widely studied power smoothing method, and efforts have been made to improve it by creating a more robust version known as the Exponential Moving Average (EMA) and Enhanced Linear Exponential (ELES). EMA and ELES are suitable for laboratory experiments due to their ability to determine the direction PV fluctuations flow [24]. Additionally, Barakat et al. [25] model a hybrid marine current and H_2 system, demonstrating that the combination of these technologies is complementary.

In summary, the literature review presented in this study reveals several gaps that need to be addressed. While the sizing optimization of an off-grid renewable system using HOMER Pro is not a novelty, controlling the SC power smoothing band to reduce power fluctuations in H_2 production using FC has not been found in the reviewed literature. Therefore, this paper presents a power smoothing method for an off-grid renewable system (PV/HKT/H_2/SC). The main objective of the new method is to control the SOC of the SC using an FC, allowing for the reduction of power fluctuations and efficient H_2 production. To generate the power signals for FC and SC, two well-known power smoothing methods, ELES and EMA are used. This study goes further by considering a hydrokinetic turbine (HKT) as backup power station, ensuring the continuity and reliability of off-grid electricity supply. This approach is relatively new, and it investigates new concepts of power smoothing using H_2, HKT, PV and SC for off-grid power systems within a technical framework. Exhaustive experiments have been conducted in a Micro-Grid laboratory at the University of Cuenca using real data. The inclusion of an efficient hydrogen storage system is of utmost importance in achieving the enhanced performance of the HRES studied in this paper. By harnessing surplus electricity during peak renewable energy production, the H_2 storage system ensures that excess energy is stored efficiently and made available during periods of low renewable generation. This real-time energy balancing not only minimizes wastage of renewable energy but also mitigates the impact of unpredictable fluctuations, enabling a smoother and more reliable power supply to meet the load demand. Moreover, the hydrogen electrolyzer and fuel cell components of the H_2 storage system play a pivotal role in maintaining the power smoothing band of the SC, ensuring that the SC's SOC remains within the predefined limits. This dynamic control strategy contributes to a more stable and continuous energy supply, particular attention is

given to the role of the SC within the HRES and how it effectively addresses crucial issues associated with PV panels. As PV panels are subject to intermittent solar irradiance and inherent variability, the SC assumes a pivotal position in managing the power fluctuations and ensuring a stable power supply to meet the load demand. By prioritizing the SC's role, this research aims to demonstrate its significance in enhancing the overall performance and reliability of the HRES.

The remainder of this document is organized as follows. Section 2 provides a description of the proposed system and outlines the laboratory used in the experiment. Section 3 details the paper's methodology, including sizing optimization and power smoothing methods, using mathematical models, simulations, and experiments. Section 4 discusses the results obtained from the technical and economic point of view. Finally, Section 5 concludes the study.

2. System overview

The connection diagram of the test bench in the laboratory is depicted in Fig. 1. The PV is linked to the direct current (DC) bus through a DC-DC converter equipped with maximum power point tracking (MPPT) capabilities. The HKT power output is converted into direct current via an AC/DC converter. To reduce power peaks generated by RES and meet demand, a SC is employed with a power smoothing band. The Elz and FC work in tandem to maintain the SC's power smoothing band within pre-established limits while simultaneously supplying power to meet the demand. In instances where the energy generated by the PV + HKT exceeds the load demand, surplus electricity is stored in the H_2 tank through the Elz. Conversely, if the PV + HKT power falls short of the load demand, the FC served an auxiliary power supply. The SC plays a crucial role in smoothing power peaks by either absorbing or delivering power during each fluctuation.

The proposed energy system includes both the advanced hydrogen storage system and the SC, which work synergistically to significantly contribute to the overall performance of the HRES. During periods of surplus renewable energy production, the H_2 storage system efficiently stores excess energy, making it available during periods of low renewable generation. This real-time energy balancing by the H_2 storage system minimizes wastage of renewable energy and mitigates the impact of unpredictable fluctuations, leading to a smoother and more reliable power supply to meet the load demand. The SC, on the other hand, plays a crucial role in maintaining power smoothing within the HRES. Its rapid response capability allows it to quickly absorb or release power, effectively managing short-term fluctuations caused by intermittent renewable energy sources. By integrating the SC into the control strategy, the HRES can optimize the utilization of renewable energy resources, ensure a stable power supply, and reduce wear and tear on other energy storage components. In summary, the inclusion of both the efficient hydrogen storage system and the SC is of utmost importance in achieving the enhanced performance and reliability of the HRES. The SC's ability to address the crucial issues of PV panels, such as power fluctuations and intermittency, helps maintain a smoother and more reliable power supply to meet the load demand. Through their combined capabilities, the energy storage systems not only reduce power fluctuations but also ensure a constant and optimized power supply, ultimately leading to improved overall system efficiency and resiliency.

3. Methodology

This paper presents a novel methodology for controlling the power smoothing band of a SC using a FC in a grid-connected HRES. The analysis is conducted from multiple perspectives. For illustrative purposes, Fig. 2 outlines the methodology employed. Initially, the capacity of the HRES is optimized using the HOMER Pro tool, which utilizes input variables typically spanning a one-year period with hourly intervals. Data on ambient temperature and solar irradiance are collected from the meteorological station at the University of Cuenca. Additionally, the river speed is determined using the HEC-RAS software from the Hydrologic Engineering Center [26], based on the optimal location of the HKT and from flow data provided by the National Institute of Meteorology and Hydrology (INAMHI) [27]. Next, the mathematical formulation serving as the basis for the modelling in the MATLAB software is presented. This section also introduces the proposed power smoothing and energy control strategies. To demonstrate the effectiveness of the power smoothing method, it is applied to the HRES optimized by HOMER Pro. To replicate the simulations experimentally, the programming is migrated to the laboratory's Supervisory Control and Data

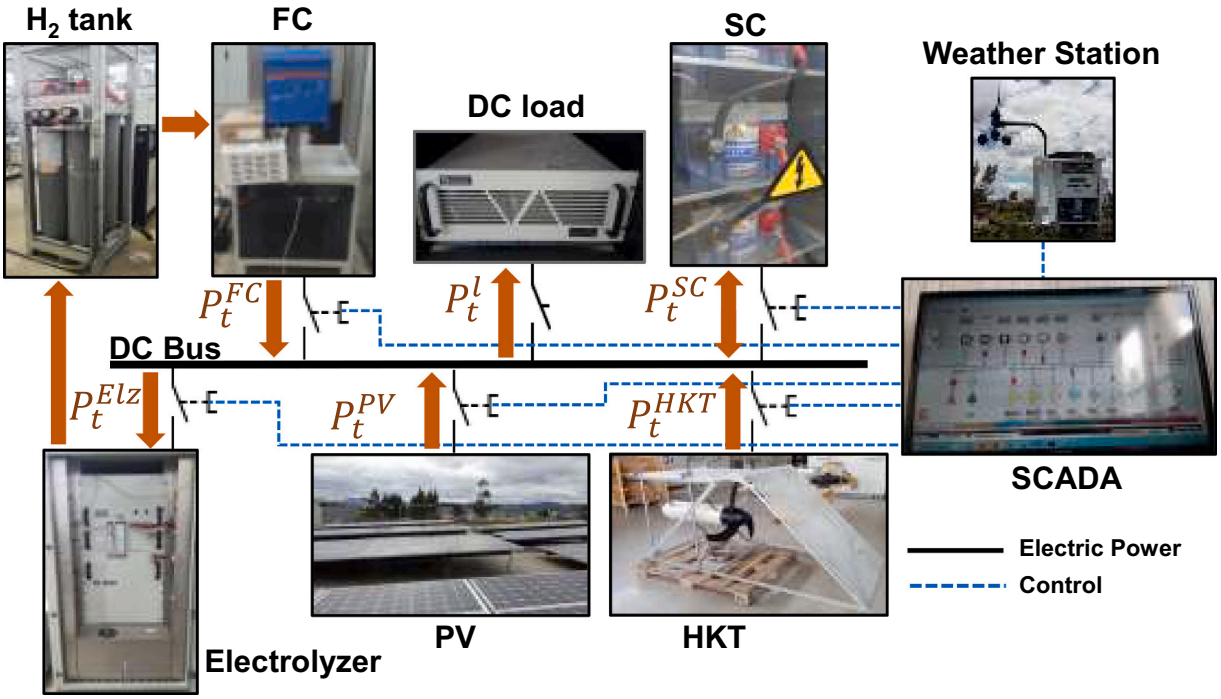

Fig. 1. Structure of PV/H_2/HKT/SC off-grid system.

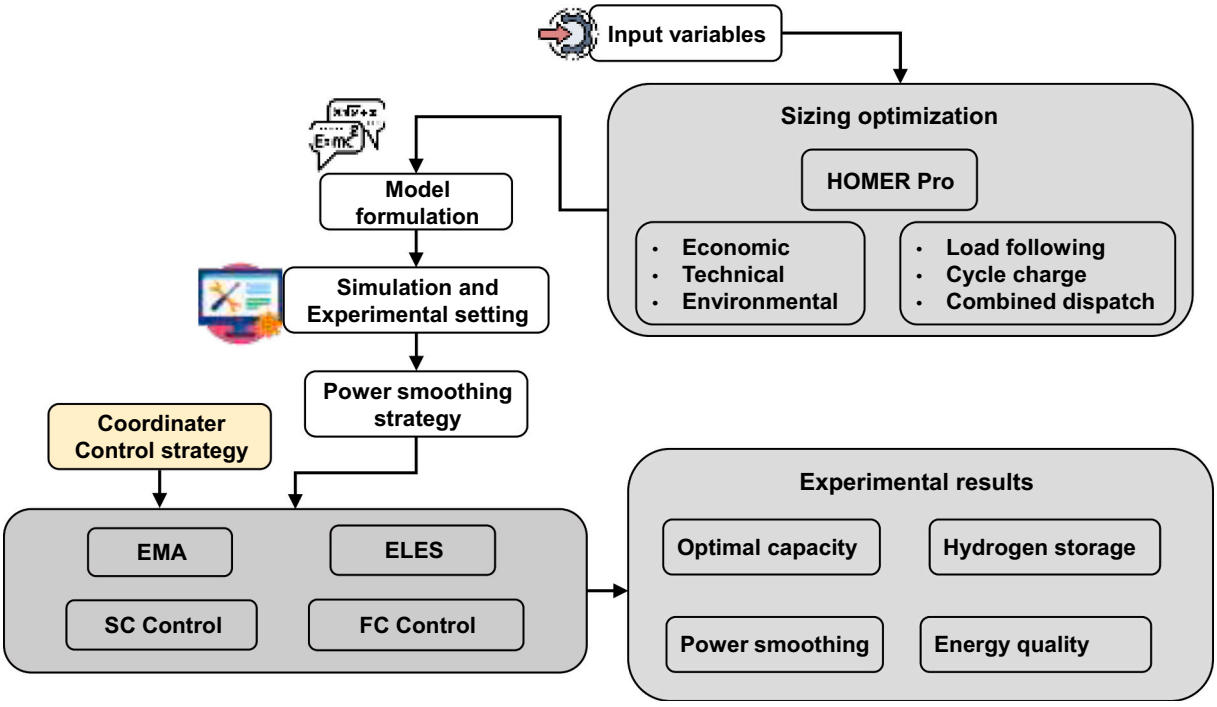

Fig. 2. Schematic representation of the proposed methodology.

Acquisition (SCADA) system. Finally, the results are comprehensively discussed from various angles, taking into consideration technical and economic indices.

3.1. Sizing optimization

HOMER Pro utilizes the input variables provided by the user to find an optimal solution, as shown in Fig. 3, which outlines the optimization process. In off-grid systems, the energy control determines the startup of the FC, the operation of SC, or both systems simultaneously based on real-time RES available.

The real input profiles data were measured in the laboratory of the University of Cuenca, as depicted in Fig. 2 of Ref. [36]. For illustrative purposes, the solar irradiance and the ambient temperature remain relatively constant throughout the year, while the electricity demand and river speed exhibit marked variations. HOMER Pro performs hundreds of thousands of simulations using the input data and selected algorithms, taking into a count cost and lifespan data. Table 1 presents the

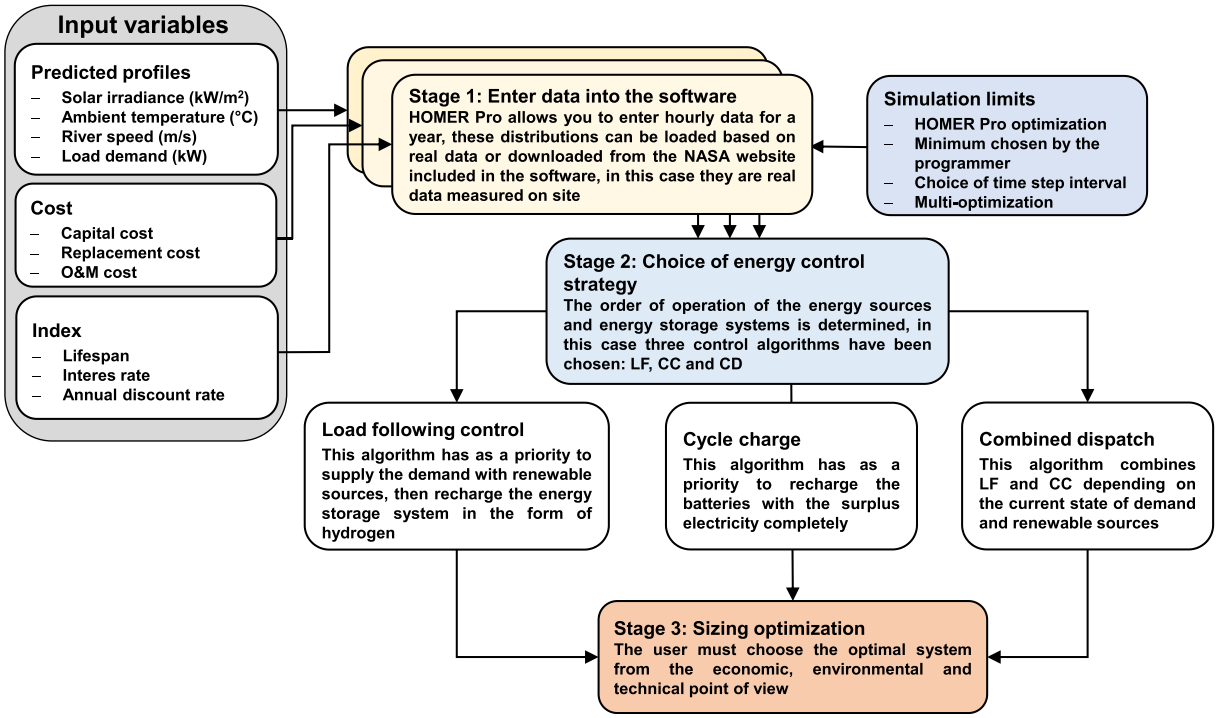

Fig. 3. Schematized HOMER Pro optimization process.

Table 1
Economic input variables to HOMER Pro of the proposed off-grid renewable system.

	Capital cost	Replacement cost	O&M cost	Lifespan	Ref.
PV	1,252 USD/kWp	484 USD/kWp	18 USD/kW/year	25 years	[31]
HKT	1,1179 USD/kW	9,876 USD/kW	10 USD/kW/year	10 years	[32]
FC	3,300 USD/kW	2,000 USD/kW	0.04 USD/op.h	40,000 h	[33]
H_2 tank	635 USD/kg	350 USD/kg	3 USD/kg/year	25 years	[33]
Elz	1,100 USD/kW	825 USD/kW	10 USD/kW/year	15 years	[34]
SC	600 USD/kW	600 USD/kW	5 USD/kW/year	30 years	[34]

main economic parameters of the HRES. The discount rate is set at 12 % [28], the inflation rate is 0.27 and the interest rate at 10 % [29]. Further details regarding equipment used for this experiment can be found in Reference [30].

3.2. Model formulation and experimental setting

In this section, the mathematical representation of the system components is used to compare and validate their behaviour with respect to the laboratory experiments. The mathematical models and experimental tests are presented in a comparative manner. For a comprehensive understanding of the laboratory used in these experiments, a detailed description can be found in Reference [30].

3.2.1. PV model

The output power of PV is show by Eq. (1) [35,36]

$$P_t^{PV} = \gamma_t^{PV}.\lambda^{PV}.\left(\frac{I_{T,t}^{PV}}{I_{S,t}^{PV}}\right).\left[1+\alpha_{pw}^{PV}.\left(T_C^{PV}-T_S^{PV}\right)\right]; \forall t \in T \cup \Xi \quad (1)$$

Constraints:

PV power flow will always be towards the DC bus, Eq. (2) must be satisfied.

$$\alpha_{pw}^{PV}.\left(T_C^{PV}-T_S^{PV}\right)\langle 1 \quad (2)$$

To avoid indeterminacy, $I_{S,c,t}^{PV} \neq 0$.where: $\gamma_{c,t}^{PV}$ is the PV rated capacity, λ^{PV} is PV derating factor (%), $I_{T,c,t}^{PV}$ is the PV current generated, $I_{S,c,t}^{PV}$ is the reverse saturation diode current, α_{pw}^{PV} is the power temperature coefficient, T_C^{PV} is the cell temperature and T_S^{PV} is the cell temperature under standard test conditions. Fig. 4(a) shows a comparison between the MATLAB simulation fitting and the real power output of the PV system extracted from the laboratory.

3.2.2. HKT model

The HKT output power is calculated by Eq. (3) [36].

$$P_t^{HKT} = P_t^{hkt}\xi_t = \left(\frac{1}{2}.\rho^{\omega}.A^{HKT}.\alpha_t^3.\zeta_p^{HKT}.\eta^{HKT}\right)\xi_t.; \forall t \in T \cup \Xi \quad (3)$$

Constraints:

ξ_t expresses output power limit considering the power curve of HKT, note Eq. (4).

$$0 \leq P_t^{HKT} \leq P_t^{HKT}\xi_t; \forall t \in T \cup \Xi \quad (4)$$

In practice, the power output is represented with Eq. (5).

$$P_t^{HKT} \leq \overline{P_t^{HKT}} \quad (5)$$

where: $P_t^{HKT}$is the total HKT power, ξ_t is the index of maximum overpower value in HKT, ρ^{ω} is the water density, A^{HKT} is the HKT sweep

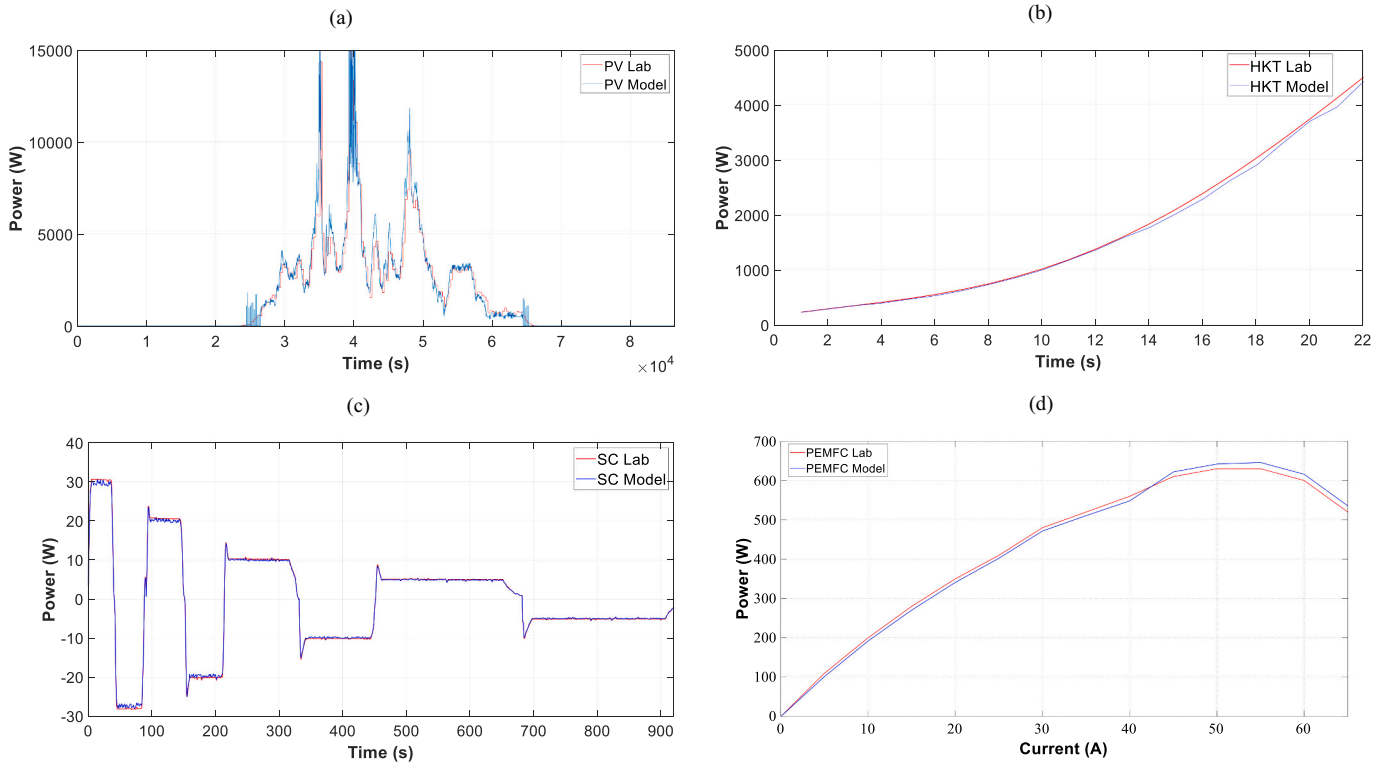

Fig. 4. Comparison of the computational model vs experiment, output electrical power: (a) PV (b) HKT (c) SC (d) FC.

surface, α_t is the river speed, ζ_p^{HKT} is the HKT power coefficient, η^{HKT} is the HKT efficiency and $\overline{P_t^{HKT}}$ is the maximum HKT power allowed. Fig. 4 (b) illustrates the output power of the mathematical model simulated in MATLAB compared to the real output power measured in the laboratory equipment.

3.2.3. SC model

The energy stored by SC is represented by Eq. (6) [37].

$$E_t^{SC} = \frac{1}{2}.C^{SC}.\left(V_t^{SC}\right)^2; \forall t \in T \cup \Xi \tag{6}$$

SOC of SC is calculated with Eq. (7) [37].

$$SOC_t^{SC} = \frac{V_t^{SC} - V_t^{min}}{V_t^{max} - V_t^{min}}; \forall t \in T \cup \Xi \tag{7}$$

Constraints

Eqs. (8) and (9) express the restrictions of the SC.

$$V_t^{min} < V_t^{SC} < V_t^{max}; \forall t \in T \cup \Xi \tag{8}$$

$$I_t^{Ch,max} < I_t^{SC} < I_t^{Dis,max}; \forall t \in T \cup \Xi \tag{9}$$

where: E_t^{SC} is the energy stored in SC (kWh), C^{SC} is the capacitance of SC in (F), V_t^{SC} is the nominal voltage in SC (V), V_t^{min} is the SC voltage lower limit (V), V_t^{max} is the SC voltage upper limit (V), $I_t^{Ch,max}$ is the maximum charge current allowed in SC (A), $I_t^{Dis,max}$ is the maximum discharge current allowed in SC (A), and I_t^{SC} is the nominal current in SC (A). Similarly, Fig. 4(c) depicts the response of the simulation and the laboratory experiment.

3.2.4. Elz model

The process of electrolysis of water to produce H_2 is represented in this section.

$$U_t^{cell} = \frac{\Delta G}{\Gamma F} + \frac{r_1 + r_2 T_{Elz}}{A^{cell}} I_t^{Elz} + \left(s_1 + s_2 T_{Elz} + s_3 T_{Elz}^2\right) log\left(\frac{t_1 + t_2 T_{Elz} + t_3 T_{Elz}^2}{A^{cell}} I_t^{Elz} + 1\right) \tag{10}$$

where: U_t^{cell} is the fuel cell voltage, ΔG is Gibbs power exchange, Γ are the transferred electrons F is Faraday constant, r_i is the resistance value of the electrolyte $(i = 1 \ldots 2)$, s_i and t_i express the overvoltage of the electrodes $(i = 1 \ldots 3)$, A^{cell} is the cell area, T_{Elz} is the electrolyte temperature and I_t^{Elz} is the DC current drawn [21].

To calculate the Elz cell voltage, Eq. (11) is used.

$$U^{Elz} = N^{Elz} U_t^{cell}; \forall t \in T \cup \Xi \tag{11}$$

where: N^{Elz} is the number of cells.

The variation of the temperature of the electrolyte during the hydrolysis process is expressed by Eq. (12).

$$C^{int,Elz} \frac{dT_t^{Elz}}{dt} = \dot{Q}_t^{fc\_gen} - \dot{Q}_t^{Elz\_loss} - \dot{Q}_t^{Elz\_cool}; \forall t \in T \cup \Xi \tag{12}$$

where: $C^{int,Elz}$is the thermal capacitance of the Elz, $\dot{Q}_t^{fc\_gen}$ represents internal heat, $\dot{Q}_t^{Elz\_loss}$ are heat losses and $\dot{Q}_t^{Elz\_cool}$ is the cooling load for auxiliary services [38]. These terms are defined by the following Eq. (13).

$$\begin{aligned} \dot{Q}_t^{fc_gen} &= N^{Elz}\left(U_t^{cell} - \frac{\Delta H}{\Gamma F}\right) I_t^{Elz}; \forall t \in T \cup \Xi \\ \dot{Q}_t^{Elz_loss} &= \frac{1}{R^{t\_Elz}}(T_{Elz} - T_a); \forall t \in T \cup \Xi \\ \dot{Q}_t^{Elz_cool} &= C^{cw}(T_{Elz} - T_{cwi})\left(1 - e^{-\frac{h^{cond} + h^{conv} \times I_t^{Elz}}{C^{cw}}}\right); \forall t \in T \cup \Xi \end{aligned} \tag{13}$$

where: ΔH is the enthalpy change, R^{t_Elz} is the Elz total thermal resistance, T_a is the ambient temperature C^{cw} is the heat capacity of the cooling water, T_{cwi} is the temperature of the inlet cooling water, h^{cond} and h^{conv} represent heat transfer by conduction and convection, respectively. The radius of H_2 production is calculated with Eq. (14) [39].

$$\dot{\eta}_{H_2} = \eta_F \frac{N^{Elz} I_t^{Elz}}{\Gamma F}; \forall t \in T \cup \Xi \tag{14}$$

where:

$$\eta_F = a_1 exp\left(\frac{a_2 + a_3 T_{Elz}}{I_t^{Elz}/A^{cell}} + \frac{a_4 + a_5 T_{Elz}}{\left(I_t^{Elz}/A^{cell}\right)^2}\right); \forall t \in T \cup \Xi \tag{15}$$

where: $\dot{\eta}_{H_2}$ is the rate of H_2 production, η_F is the faraday efficiency, a_i represent the efficiency of the Faraday ratio $(i = 1 \ldots 5)$.

3.2.5. FC model

The voltage at the FC terminals is calculated with Eq. (16) [40].

$$V_t^{FC} = N^{FC}\left(E_t^{nernst} - V_t^{act} - V_t^{ohm} - V_t^{con}\right); \forall t \in T \cup \Xi \tag{16}$$

where: E_t^{nernst} is the equilibrium voltage, V_t^{act} is the activation voltage, V_t^{ohm} is the ohmic voltage, V_t^{con} is the concentration voltage, V_t^{FC} is the FC cell voltage, N^{FC} is the number of cells. These values are calculated with the following Eq. (17).

$$\begin{aligned} E_t^{nernst} &= \frac{\Delta G}{\Gamma F} + \frac{\Delta S}{\Gamma F}\left(T_t^{FC} - T_t^{ref}\right) + \frac{RT_t^{FC}}{\Gamma F}\left[ln(P_{H_2}) + \frac{1}{\Gamma} ln(P_{O_2})\right]; \forall t \in T \cup \Xi \\ V_t^{act} &= \varsigma_1 + \varsigma_2 T_t^{FC} + \varsigma_3 T_t^{FC} ln(C_{O_2}) + \varsigma_4 T_t^{FC} ln\left(I_t^{FC}\right); \forall t \in T \cup \Xi \\ V_t^{ohm} &= I_t^{FC} R^{ohm} = I_t^{FC}(R^m + R^c) = I_t^{FC}\left(r^m l/A + R^c\right); \forall t \in T \cup \Xi \\ V_t^{con} &= -\beta ln\left(1 - \frac{\psi}{\psi_{max}}\right); \forall t \in T \cup \Xi \end{aligned} \tag{17}$$

where: ΔS is the molar entropic variation in standard conditions, T_t^{ref} is the cell reference temperature, T_t^{FC} is the temperature of FC (K), R represent the constant of the gas, P_{H_2} is the H_2 partial pressure, P_{O_2} is the effective partial pressure of oxygen, xi $(i = 1, \ldots, 4)$ are the coefficients from the thermodynamic model, I_t^{FC} is the current of FC, C_{O_2} is the oxygen concentration, R^{ohm} is the algebraic sum of the resistances, R^m is the equivalent impedance, R^c is the contact resistance between the membrane and the electrodes, r^m is the resistivity of the membrane, l is the membrane thickness, A is the membrane activation area, β is the constant determined by the FC, ψ is the current density, ψ_{max} is the maximum allowable current density [42].

The FC mole balance equations are calculated with Eq. (18) [41].

$$\begin{aligned} \frac{dP_{H_2}}{dt} &= \frac{RT_t^{an}}{V_t^{an}}\left(\dot{m}_{H_2}^{in} - \dot{m}_{H_2}^{react} - \dot{m}_{H_2}^{out}\right); \forall t \in T \cup \Xi \\ \frac{dP_{O_2}}{dt} &= \frac{RT_t^{ca}}{V_t^{ca}}\left(\dot{m}_{O_2}^{in} - \dot{m}_{O_2}^{react} - \dot{m}_{O_2}^{out}\right); \forall t \in T \cup \Xi \end{aligned} \tag{18}$$

where: T_t^{an} is the temperature of the gas accumulation in the anode, V_t^{an} is the volume of the anode, $\dot{m}_{H_2}^{in}$ is the H_2 inlet mass flow rate, $\dot{m}_{H_2}^{react}$ is the H_2reaction mass flow rate, $\dot{m}_{H_2}^{out}$ is the outlet mass flow rate of H_2, T_t^{ca} is the gas temperature in cathode, V_t^{an} is the cathode control volume, $\dot{m}_{O_2}^{in}$ is the oxygen inlet mass flow rate, $\dot{m}_{O_2}^{react}$ is the reaction oxygen mass flow rate, $\dot{m}_{O_2}^{out}$ is the oxygen output mass flow rate.

Therefore, the general energy equation of FC is:

$$Q^{stack} = \dot{Q}^{FC\_gen} - P^{FC} - \dot{Q}^{FC\_cool} - \dot{Q}^{FC\_loss}; \forall t \in T \cup \Xi$$
$$C^{t\_FC} \times \frac{dT_t^{FC}}{dt} = Q^{stack}; \forall t \in T \cup \Xi \quad (19)$$

where: C^{t_FC} is the thermal capacitance of the FC, $\dot{Q}^{FC\_gen}$ is the heat generated by the chemical reaction of energy conversion, P^{FC} is the electricity produced by FC, $\dot{Q}^{FC\_cool}$ is the amount of energy for cooling, $\dot{Q}^{FC\_loss}$ are losses. These parameters are calculated with the Eq. (20) [42].

$$\dot{Q}^{fc\_gen} = \dot{m}_{H_2}^{react} \Delta H = \frac{N^{FC} I_t^{FC}}{\Gamma F} \Delta H; \forall t \in T \cup \Xi$$
$$P_t^{FC} = V^{stack} I_t^{FC} = N^{FC} V_t^{FC} I_t^{FC}; \forall t \in T \cup \Xi$$
$$\dot{Q}^{FC\_cool} = \left(h^{cond} + h^{conv} \times I_t^{FC}\right) \frac{\left(T_t^{FC} - T_t^{cwi}\right) - \left(T_t^{FC} - T_t^{cwo}\right)}{ln\left[\left(T_t^{FC} - T_t^{cwi}\right)/\left(T_t^{FC} - T_t^{cwo}\right)\right]}; \forall t \in T \cup \Xi$$
$$\dot{Q}^{FC\_loss} = \frac{T_t^{FC} - T_t^{a}}{R^{t\_FC}}; \forall t \in T \cup \Xi \quad (20)$$

where: N^{FC} is the number of cells connected in series within FC, V^{stack} is the voltage in FC terminals, T_t^{cwo} is the outlet cooling water temperature, R^{t_FC} is the overall thermal resistance of the FC. In this sense, Fig. 4(d) displays the behaviour of the electrical power in relation to the fuel cell (FC) current, comparing the modelling results with the experimental data.

3.3. Electric power flow balance

The primary objective of the HRES power flow is to ensure the supply meets the demand, reducing unmet load and handling surplus electricity. In cases of insufficient RES, the H_2 system acts as a backup support the load demand. The SC is mainly responsible for reducing power fluctuations but can energetically supply the demand in emergent conditions. The power flow equations governing the proposed HRES are described below:

$$P_t^l = \left[\left(P_t^{PV} + P_t^{HKT}\right) - \left(P_t^{FC} + P_t^{SC}\right)\right] \; If \left[\begin{cases} \left(P_t^{HKT} + P_t^{PV}\right) \geq P_t^l \\ SOC_t^{SC} \leq SOC_{min,t}^{SC} \\ SOC_t^{H_2} \leq SOC_{min,t}^{H_2} \end{cases}\right]; \forall t \in T \cup \Xi \quad (21)$$

$$P_t^l = \left[\left(P_t^{PV} + P_t^{HKT}\right) - \left(P_t^{FC} - P_t^{SC}\right)\right] \; If \left[\begin{cases} \left(P_t^{HKT} + P_t^{PV}\right) \geq P_t^l \\ SOC_t^{SC} > SOC_{min,t}^{SC} \\ SOC_t^{H_2} \leq SOC_{min,t}^{H_2} \end{cases}\right]; \forall t \in T \cup \Xi \quad (22)$$

$$P_t^l + P_t^{SC} = \left[\left(P_t^{PV} + P_t^{HKT}\right) - \left(-P_t^{FC}\right)\right] \; If \left[\begin{cases} \left(P_t^{HKT} + P_t^{PV}\right) \geq P_t^l \\ SOC_t^{SC} \leq SOC_{min,t}^{SC} \\ SOC_t^{H_2} > SOC_{min,t}^{H_2} \end{cases}\right]; \forall t \in T \cup \Xi \quad (23)$$

$$P_t^l = \left[\left(P_t^{PV} + P_t^{HKT}\right) - \left(-P_t^{FC} - P_t^{SC}\right)\right] \; If \left[\begin{cases} \left(P_t^{HKT} + P_t^{PV}\right) \geq P_t^l \\ SOC_t^{SC} > SOC_{min,t}^{SC} \\ SOC_t^{H_2} > SOC_{min,t}^{H_2} \end{cases}\right]; \forall t \in T \cup \Xi \quad (24)$$

$$P_t^l = \left[P_t^{FC} + P_t^{SC}\right] \; If \left[\begin{cases} \left(P_t^{HKT} + P_t^{PV}\right) \langle P_t^l \\ SOC_t^{SC} > SOC_{min,t}^{SC} \\ SOC_t^{H_2} > SOC_{min,t}^{H_2} \end{cases}\right]; \forall t \in T \cup \Xi \quad (25)$$

$$P_t^l + P_t^{SC} = P_t^{FC} \; If \left[\begin{cases} \left(P_t^{HKT} + P_t^{PV}\right) \langle P_t^l \\ SOC_t^{SC} \leq SOC_{min,t}^{SC} \\ SOC_t^{H_2} > SOC_{min,t}^{H_2} \end{cases}\right]; \forall t \in T \cup \Xi \quad (26)$$

$$P_t^l = P_t^{SC} \; If \left[\begin{cases} \left(P_t^{HKT} + P_t^{PV}\right) \langle P_t^l \\ SOC_t^{SC} > SOC_{min,t}^{SC} \\ SOC_t^{H_2} \leq SOC_{min,t}^{H_2} \end{cases}\right]; \forall t \in T \cup \Xi \quad (27)$$

$$P_t^l = unmet\ load \; If \left[\begin{cases} \left(P_t^{HKT} + P_t^{PV}\right) \langle P_t^l \\ SOC_t^{SC} \leq SOC_{min,t}^{SC} \\ SOC_t^{H_2} \leq SOC_{min,t}^{H_2} \end{cases}\right]; \forall t \in T \cup \Xi \quad (28)$$

In summary, the energy flow algorithm is visually explained in Fig. 5, where: $P_t^{PV}, P_t^{HKT}, P_t^{FC}, P_t^{SC}$ are the output powers of PV, HKT, FC and SC respectively, P_t^l is the electricity demand; $SOC_t^{SC}, SOC_{min,t}^{SC}, SOC_t^{H_2}, SOC_{min,t}^{H_2}$ are the nominal SOC of SC and the H_2 tank, respectively.

3.4. Power smoothing methodology

The power smoothing method proposed in this paper utilizes a combination of SC and FC. SC absorbs faster power fluctuations, while long-term variations are directed to FC. The Eqs. (23) and (26) explain the energy flow under these conditions. If the SC's SOC falls below the minimum threshold, FC operates at full load to bring the SC to safe SOC levels. Conversely, if the SC's SOC exceeds the high limit, the Elz absorbs surplus electricity by reducing the SC's charge to predetermined values. Therefore, the power smoothing algorithm requires a reference power, which in this case depends on the HRES conditions to define the producing component of this reference. The new proposed method is centered on controlling the SC's power smoothing band using FC. For this purpose, reference signals are generated using two conventional power smoothing methods: EMA and ELES, as show in Fig. 6(a), and the obtained results are compared. Power smoothing will effectively reduce power peaks in the operation of the Elz.

3.4.1. Exponential moving average method

The EMA power smoothing strategy calculates the reference power $P_{ref,t}^{HRES}(k)$ for the proposed power smoothing method and is activated when fluctuations exceed the defined ramp rate (10 %/min). The reference is calculated using Eq. (29) [43,44]:

$$P_t^{EMA}(k) = \sum_{n=0}^{w-1} \alpha\left[(1-\alpha)^n P_t^{HRES}(k-n)\right] - P_t^{HRES}(k); \forall t \in T \cup \Xi \quad (29)$$

where n = {0, 1, 2, …, w - 1}, α represents the power smoothing coefficient.

3.4.2. Enhanced linear exponential smoothing method

The reference power calculated through the ELES method is mathematically expresses using Eq. (30). The ELES method requires a minimum energy storage capacity to mitigate the same level of power variation [45]:

$$P_t^{ELES} = \varrho P_{HRES}^{'}(t) + (1-\varrho) P_{HRES}^{'}(t-1); \forall t \in T \cup \Xi \quad (30)$$

where ϱ is the smoothing factor [0-1].

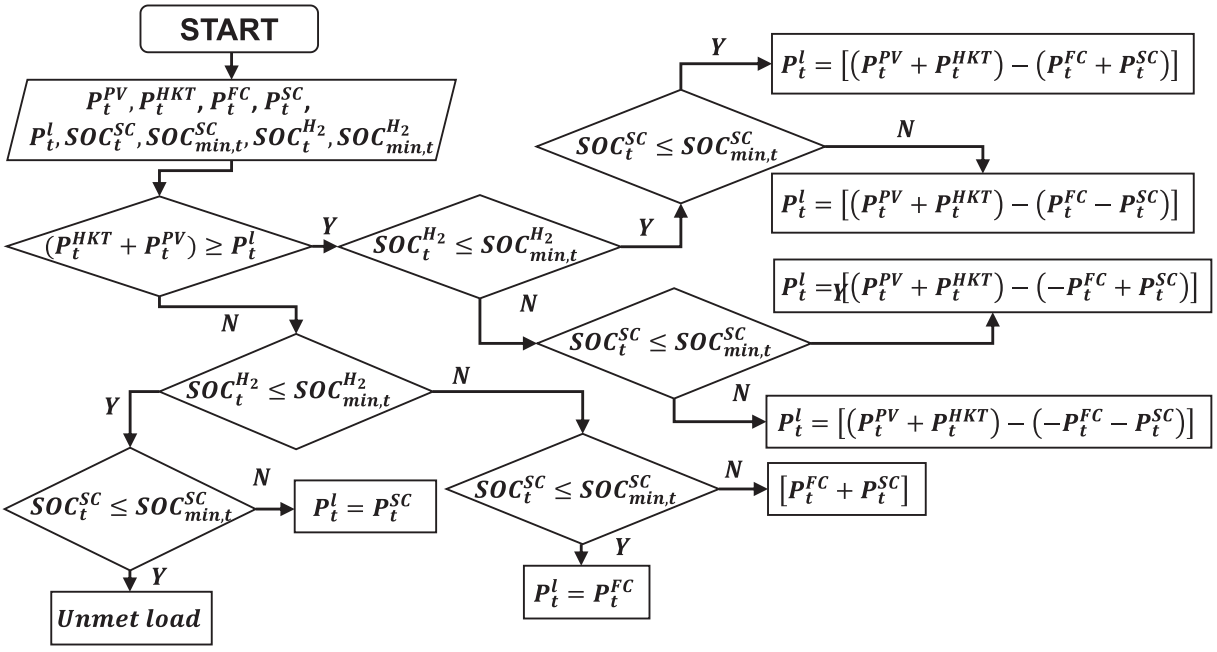

Fig. 5. Schematic representation of the power flow balance for the off-grid HRES.

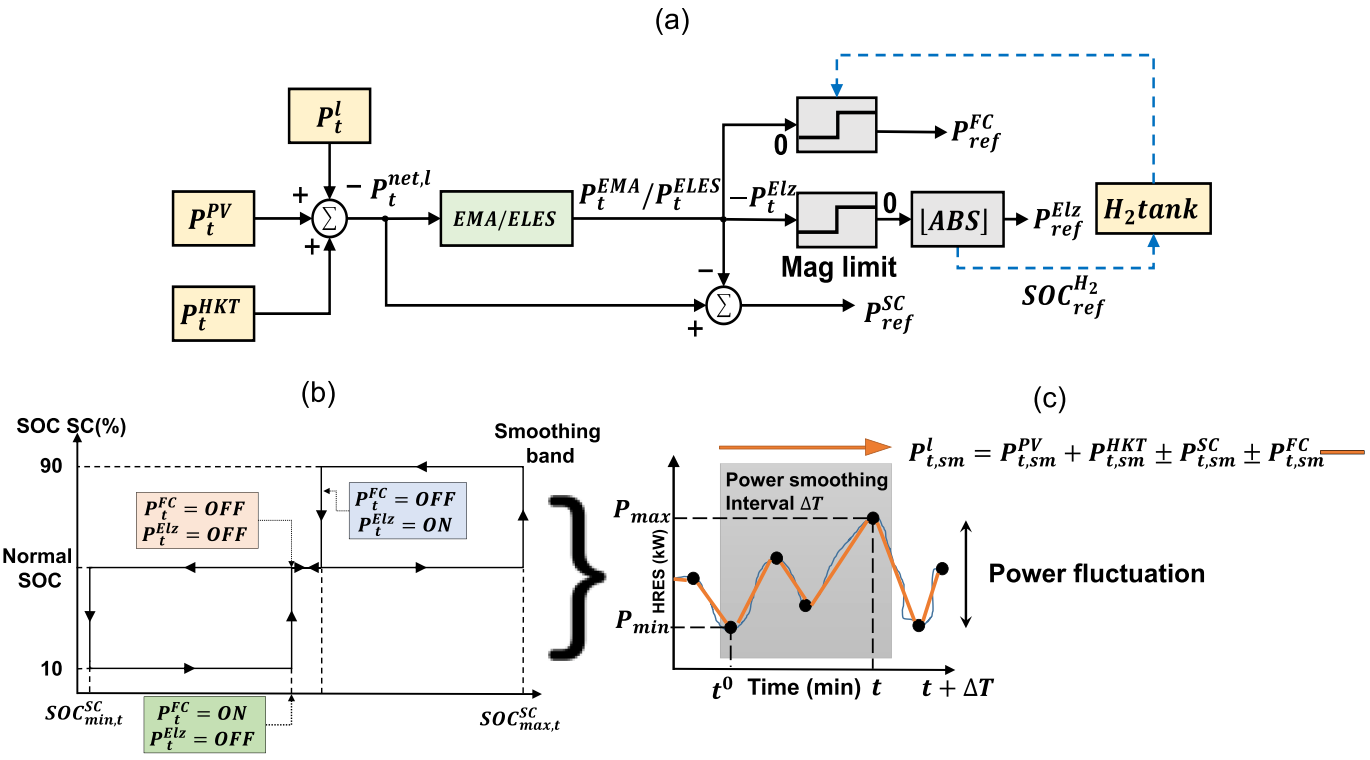

Fig. 6. (a) Reference power generation of HRES. (b) Power smoothing band control. (c) Time window used for power smoothing analysis.

3.4.3. *Control of power smoothing band and reference signals*

Fig. 6(a) illustrates the control scheme proposed to generate the reference signals. The net power $\left(P_t^{net,l}\right)$ fed into the power smoothing method comprises power fluctuations from RES and the load demand. The smoothed power output, depending on the method used $\left(P_t^{EMA}$ or $P_t^{ELES}\right)$, is used to generate the FC and Elz reference signals $\left(P_{ref}^{FC}$ and $P_{ref}^{Elz}\right)$. It's important to note that these two signals cannot be generated simultaneously; it depends on the instantaneous state of the HRES. On the other hand, the smoothed signals are subtracted from the net power to obtain the reference power of the SC $\left(P_{ref}^{SC}\right)$. The power smoothing band in the SC is defined as $\left(SOC_{min,t}^{SC} < SOC_t^{SC} < SOC_{max,t}^{SC}\right)$. In the laboratory's SC bank inverter, a minimum SOC of 5 % and a maximum SOC of 95 % are required. However, to prevent overexertion in the equipment, a minimum SOC of 10 % and a maximum SOC of 90 % are imposed.

The SOC control ensures that the SC stays within the power smoothing band. The energy flow equations guarantee the continuity of the electrical service, while the SC and the H_2 system improve energy quality by reducing power fluctuations, as shown in Fig. 6(b). The SC absorbs power peaks by charging or discharging, depending on the scenario, while the FC and Elz work together to keep the SC within its power smoothing band. The FC will operate at full load to supply the demand and/or charge the SC, depending on the HRES conditions. Similarly, the Elz operates to absorb surplus electricity and/or discharge the SC, depending on the energy conditions system.

3.4.4. Input variables and time interval

The time window for the power smoothing analysis differs from the HRES sizing because power fluctuations occur at minute intervals, as depicted in Fig. 6(c). In this section, the analysis is conducted for a randomly selected day with minute time step, specifically for June days. Therefore, the input variables are illustrated in Fig. 4 of Ref. [36], where two days with different characteristics of solar irradiance, river speed, ambient temperature, and electricity demand are chosen for the analysis.

4. Results and discussion

This section presents the experimental and simulation results of the proposed method. Firstly, the size optimization results using HOMER Pro based on economic and technical indices are discussed. Then, the results of the power smoothing method applied to the previously optimized HRES are presented, and technical criteria such as net power, SOC, H_2 storage, Elz operability are evaluated. Finally, several sensitivity analyses are conducted to verify the power smoothing results with greater precision. The fluctuation suppression rate and mean SOC are evaluated under different HRES configurations.

4.1. Sizing optimization results

The optimal configuration for the HRES is determined using the optimization software HOMER Pro [46]. This widely-used tool simulates viable systems by considering all possible combinations of equipment, resulting in hundreds or even thousands of potential systems. For this study, it has been simulated for a period of one year using real data with a time step of 1 h. The type of energy control cycle charging (CC), load following (LF) and combined dispatch (CD) is chosen. The result is shown in Table 2. The optimization range is sufficiently large enough that HOMER Pro finds the best possible solution. Among the different energy control strategies, LF energy control has yielded the most optimal solution. Despite the peak demand being around 20 kW, the sizing of PV and HKT systems is doubled, as hourly data for an entire year reveals periods with limited solar irradiance and river speed. Therefore, the H_2 system must ensure a continuous supply electricity with a 30 kg capacity of H_2 tank to meet the energy demands during these less favourable periods.

HOMER Pro optimizes the off-grid HRES to achieve the lowest cost while ensuring uninterrupted electricity supply. The annual energy production of each component is displayed in Table 3. The results demonstrate that the surplus electricity is considerably higher than the unmet load. It is possible to reduce these indices by increasing the energy cost, as observed in the simulations. However, in this case, the option recommended by the HOMER Pro software has been selected, as it provides a balanced and cost-effective solution for the HRES. This ensures a reliable and efficient power supply while minimizing overall expenses.

Table 2
Sizing optimization with HOMER Pro of the proposed HRES.

Component	Optimal capacity	Optimization range	Control algorithm
PV	40 kW	0 kW – 100 kW	LF
HKT	40 kW	0 kW – 100 kW	LF
FC	10 kW	0 kW – 100 kW	LF
Elz	30 kW	0 kW – 100 kW	LF
H_2Tank	30 kg	0 kg – 100 kg	LF
SC	165 F	0 F – 500 F	LF

Table 3
Electrical summary.

Surplus electricity and Unmet load		
Quantity	Value	Units
Surplus electricity	33,225	kWh/y
Unmet load	3649	kWh/y
Capacity shortage	4452	kWh/y
Production summary	Production (kWh/y)	Percent (%)
PV	61,913	44.1
HKT	65,394	46.6
FC	13,157	9.37
Total	140,463	100
Consumption summary	Production (kWh/y)	Percent (%)
Load demand	69,351	65.8
Deferrable load	0	0
Total	105,465	100

The primary objectives of the H_2 system are to maintain the SC within its defined power smoothing band and to supply the electricity demand in the case the RES are unable to meet the load demand. In this regard, Fig. 7(a) illustrates the hourly SOC of the H_2 tank over the course of a year. The H_2 tank experiences two instances where it is discharged to minimum levels, while for the rest of the days, the control system ensures that there is sufficient H_2 to keep the SC within its power smoothing band. The total stored capacity of the H_2 tank exceeds 1000 kWh with an autonomy of 120 h. The H_2 system's initial content is 20 kg and by the end of the year, it reaches 26.4 kg. The total H_2 consumed during the year is 782 kg, with an average consumption of 2.4 kg per day. It is essential to mention that H_2 loads have not been considered in this paper, which could be a suitable approach to utilize of surplus electricity effectively. The operation of the Elz is depicted in Fig. 7 (b). The component has been enabled for 2991 h per year with a capacity factor of 13 %. This demonstrates the Elz's functionality and effectiveness in converting electricity to hydrogen for storage and subsequent use in the fuel cell to manage power fluctuations and ensure smooth electricity supply.

4.2. Economic analysis

The economic analysis is based on the data provided in Table 1, considering a discount rate of 12 %, an inflation rate of 0.27 and an interest rate 10 % for period of 25 years. Utilizing this data, HOMER Pro calculates the Net Present Cost (NPC) and Levelized Cost of Electricity (LCOE) for the optimized configuration [47]. The NPC is calculated to be USD 210,563, resulting in an LCOE is 0.19 USD/kWh. Graphically, Fig. 8 (a) shows the economic results of the HRES. It is evident that the capital cost is high, the PV component representing the highest cost followed by the Elz. However, the operating cost is relatively lower as the HRES mainly relies on RES that require minimal and cost-effective maintenance. The salvage value is also low, considering that H_2 technologies are still in the development stage and involves high costs. The low LCOE is attributed to the participation of PV and HKT which contribute to lower energy production costs. Additionally, Fig. 8(b) displays the cash flow results, indicating a decrease in the overprice of H_2 over time. The integration of RES in the HRES leads to manageable and low prices, and the recovery period is shortened due to the penetration of RES in the system. This suggests that the HRES becomes more economically viable and cost-effective as time progresses.

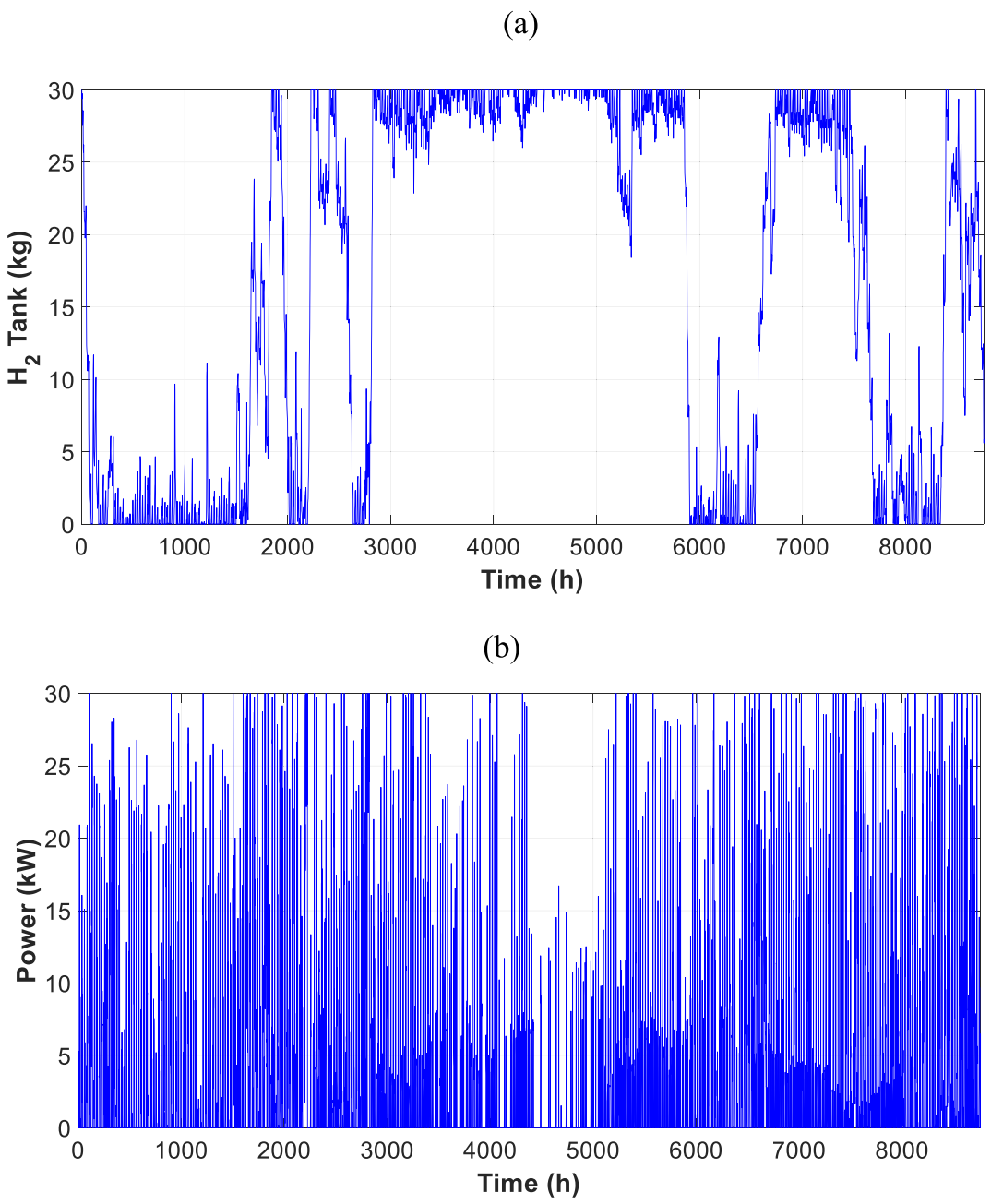

Fig. 7. (a) Stored H_2 consumption (kg/min) (b) Elz input power (kW).

4.3. Power smoothing results

To validate the proposed power smoothing method, extensive experiments were conducted in the laboratory setup as shown in Fig. 1. The data and parameters of the system, including technical specifications of the equipment used, were considered based on the datasheet provided in Reference [34]. The net power signal, denoted as ($P_t^{net.l} = P_t^{PV} + P_t^{HKT} - P_t^{l}$), as shown in the control diagram of Fig. 6(a), determines the operation of the FC or Elz based on the power flow. This fluctuating signal passes through the power smoothing algorithms (EMA/ELES), and the resulting reference signals, (P_t^{EMA}/P_t^{ELES}), activate the H_2 system. The response of the power smoothing method applied to the net power signal $\left(P_t^{net.l}\right)$ presented in Fig. 9(a). The EMA method effectively averages the power peaks, reducing the maximum values. On the other hand, the reference signal generated by the ELES method maintains the power peaks without reducing values >10 %/min. In response to any deficit of renewable power, the H_2 system supplies electricity through the FC. Fig. 9(b) displays the SOC of the H_2 tank, with the power smoothing methods effectively reducing the depth of H_2 discharge, although the impact is negligible.

Similarly, Fig. 9(c) illustrates the smoothing of net power for day two. The net power output is effectively smoothed, the EMA method averaging power fluctuations and the ELES method retaining the random nature of power. Moreover, Fig. 9(d) presents the response of the H_2 system, where the difference becomes more evident. Applying the power smoothing method with the reference signal generated by EM results in a lower depth of discharge of the H_2 tank. Power fluctuations, arising from RES and demand, are reflected in the production of H_2, and surplus electricity activates the Elz, storing H_2 in the tank. The results of power smoothing using two proposed methods are shown in Fig. 10. The averaging of power fluctuations by EMA method causes an offset of the

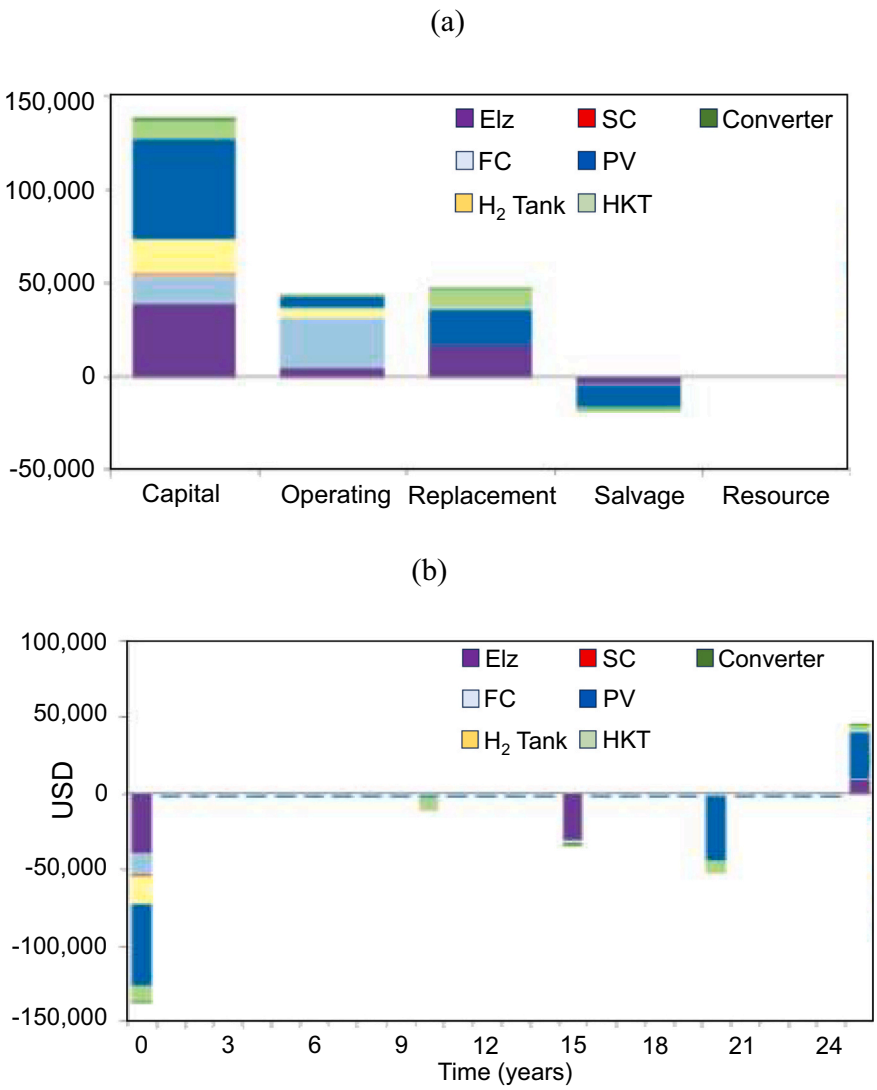

Fig. 8. (a) Cost summary of HRES proposed (b) Cash flow of HRES proposed.

upper and lower values, as displayed in Fig. 10(a). This result reduces the power fluctuations in the Elz during H_2 production, due to the effect of the SC. Such a result is promising since an off-grid system lacks a robust reference signal to facilitate smooth operation of the Elz, and fluctuations in power would generate dynamic stresses on the H_2 system in the absence of the power smoothing algorithm. Additionally, the operation of SC is smoother using the EMA algorithm, as depicted in Fig. 10(b). The H_2 system controls SOC of SC, keeping the power smoothing band within the established limits, and enables the Elz to reduce the upper value or the FC to charge the SC, increasing the lower value of its SOC.

A similar behaviour is observed for day two, as shown in Fig. 10(c) and (d). For this analyzed time interval, the SOC of the SC remains at high levels. When renewable production is insufficient to meet the demand and the H_2 storage is limited, the SC supplies the load demand. The effect of the SC reduces power fluctuations in the Elz, this result confirming the results obtained for day one and demonstrating the correct operation of the proposed power smoothing method. An improvement in H_2 production has been noted, as evidence in the results for day two is shown in Fig. 10(d). The initial SOC of the SC is approximately 50 %, as the power control maintains the SOC fully charged at the beginning of the analysis period (365 days). Therefore, for the analyzed June days, the SOC remains at approximately 50 %.

The results obtained for the days under study demonstrate the effectiveness of the proposed power smoothing method. To assess the method's performance over a longer interval, Fig. 11(a), present a global result for a sample interval of 8760 h (the whole year). It is evident that the H_2 storage exhibits a smooth behaviour over the year when applying both the ELES and EMA methods. This improvement in H_2 production through the Elz is consistent over the long-term interval, indicating the sustained effectiveness of the power smoothing method. Fig. 11(b) displays the response of the FC, showing that applying the proposed method with EMA and ELES, the FC reduces its maximum levels of operation. While this reduction may seem low for individual instances, considering a long-term interval, the overall impact becomes notable. The power smoothing method successfully controls and reduces the FC's operation, leading to improved efficiency and less stress on the FC component. Finally, Fig. 11(c) shows the SOC of the SC. As proposed, the energy control maintains the SOC within the defined power smoothing band throughout the year effectively utilizing FC to achieve this control. The SC remains within the established limits, ensuring smooth and efficient operation and contributing to the reduction of power fluctuations in the overall system.

Overall, the results presented in Fig. 11 demonstrate the consistent and beneficial effects of the proposed power smoothing method over extended time intervals, confirming its effectiveness in maintaining

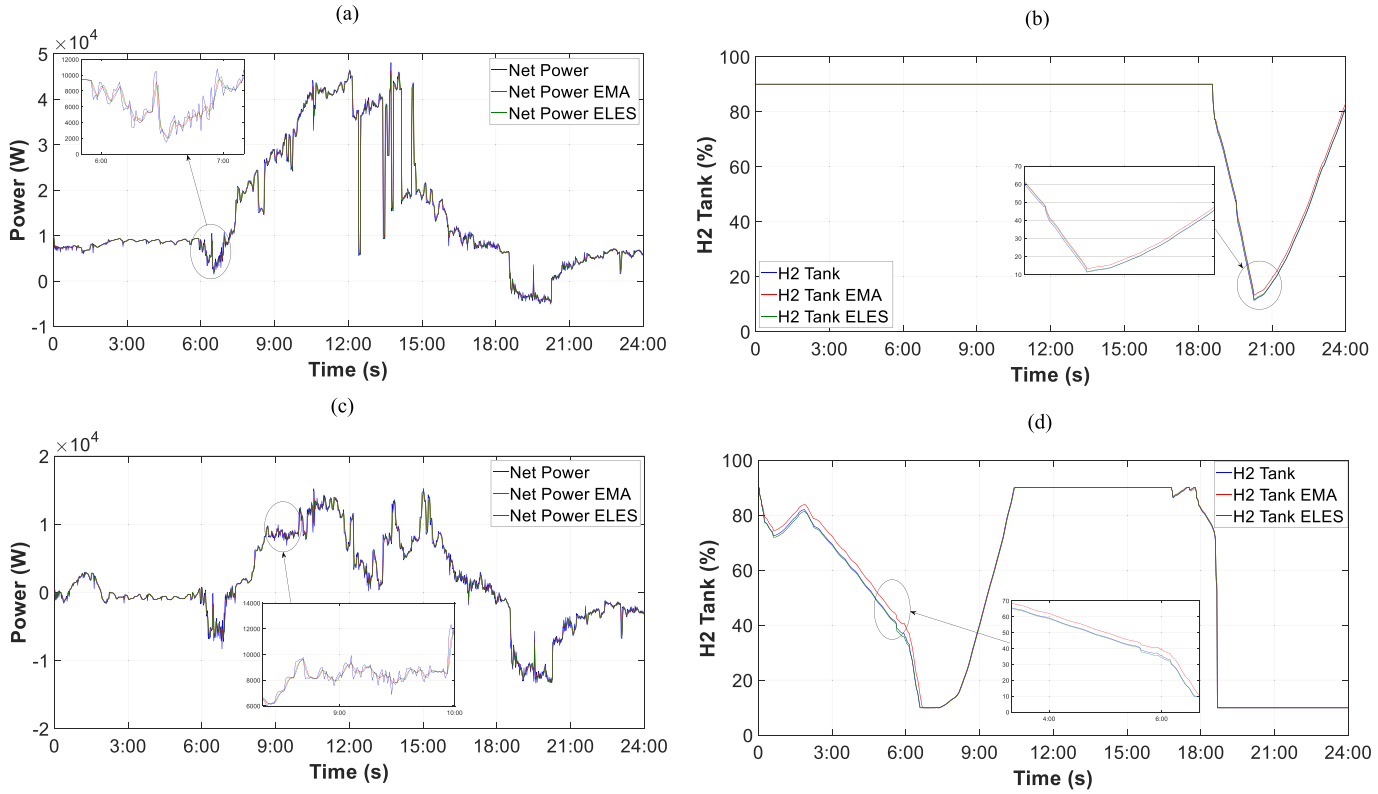

Fig. 9. Comparative results using EMA/ELES to generate the reference signals for day one: (a) Net power output. (b) State of charge of the H_2 tank. For day two: (c) Net power output. (d) State of charge of the H_2 tank.

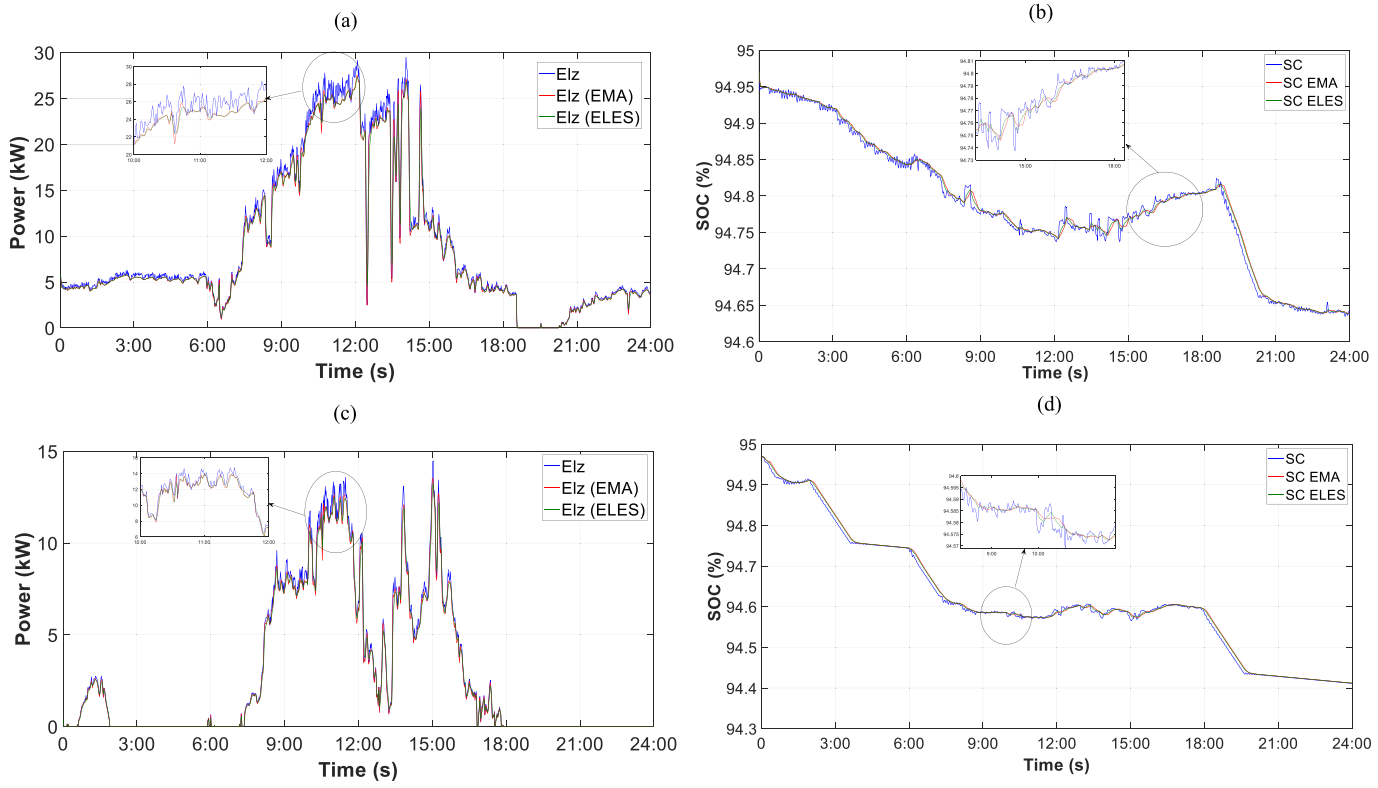

Fig. 10. H_2 production with surplus electricity: Day one (a) Elz power output and (b) SC state of charge; And day two (c) Elz power output and (d) SC state of charge.

(a)

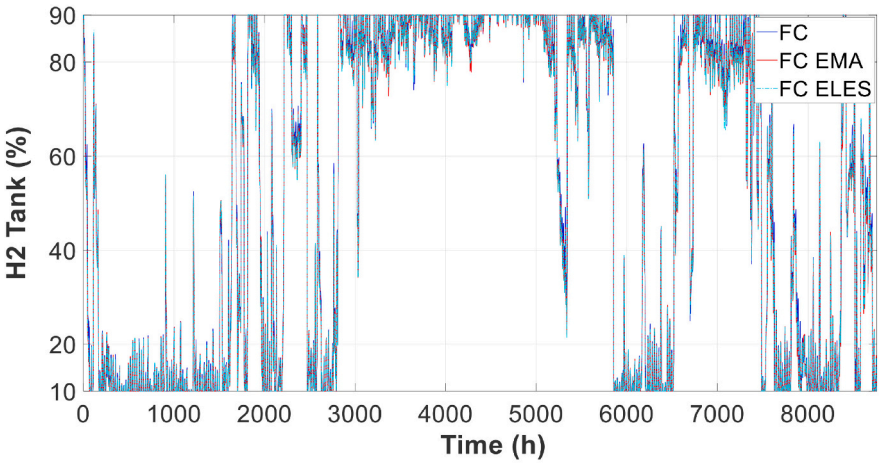

(b)

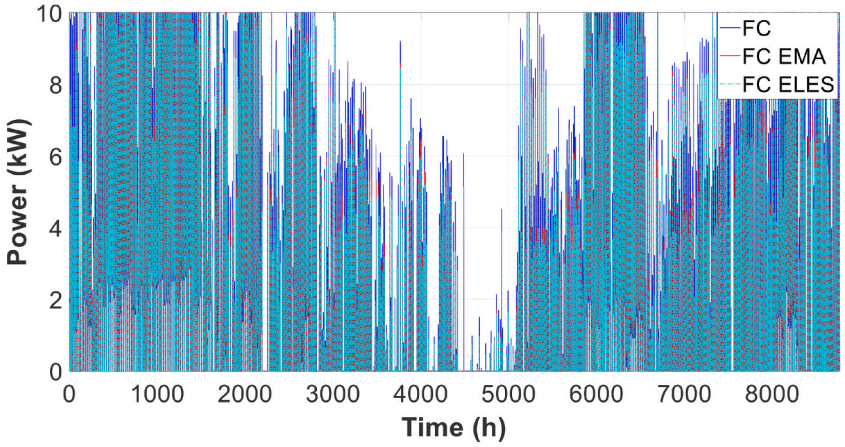

(c)

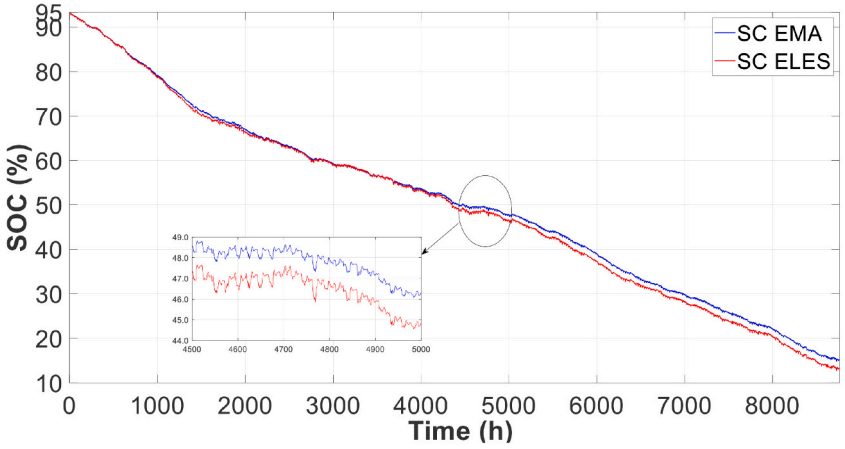

Fig. 11. Annual result of the proposed power smoothing method: (a) Output power of the electrolyser (b) Output power of FC (c) State of charge of the SC.

stable power supply and enhancing the performance of the HRES. The experimental results demonstrate that by giving priority to the SC, the HRES effectively manages and mitigates the challenges associated with PV panels. The SC's rapid response to PV power fluctuations ensures a constant and stable energy supply, enhancing the system's resilience to variability in solar irradiance. Additionally, by efficiently smoothing out power fluctuations, the SC reduces the wear and tear on other components, prolonging the overall system's lifespan and reducing maintenance costs.

4.4. Sensitivity analysis

4.4.1. Fluctuation suppression rate (FSR) [%]

The FSR is expressed as a percentage and provides an indication of how effectively the power smoothing method reduces the amplitude of power fluctuations in the net load. Higher FSR values indicate better performance in reducing power fluctuations and enhancing the stability of the off-grid system. It is calculated using the following Eq. (31) [23]:

$$FSR = \frac{\sum_{i=SP}^{FP}\left(M_{ti} \times P_{ti}^{SC}\right)}{\sum_{i=SP}^{FP}\left(M_{ti} \times P_{ti}^{net,l}\right)}; \forall t \in T \cup \Xi \tag{31}$$

where: SP and FP are the start point and finish point of the loop respectively, M_{ti} it is the fluctuation control mode (EMA or ELES) at instant i of the period of interest and is activated when the ramp exceeds 10 %/min, otherwise its value is 0.

4.4.2. Mean SOC (MSOC) [%]

The MSOC is expressed as a percentage and provides insight into how well the power smoothing method controls and maintains the SC's state of charge within the defined power smoothing band. Higher MSOC values indicate better performance in maintaining the SC's state of charge within the desired range, ensuring more effective power smoothing and system stability over time., the MSOC can be calculated with Eq. (32) [23]:

$$MSOC = \frac{\sum_{i=SP+1}^{FP}\left(SOC_{ti}^{SC} - SOC_{offset}^{SC}\right) \times \Delta T}{\sum_{i=ST}^{FP}\left(SOC_{ti}^{SC} - SOC_{offset}^{SC}\right) \times (FP - SP) \times \Delta T}; \forall t \in T \cup \Xi \tag{32}$$

where: ΔT is the sampling period.

The results in Table 4 show the MSOC values for both Day one and Day two when applying the power smoothing methods (EMA and ELES) and the FSR values for the FC and Elz with respect to the HRES without power smoothing. The average SOC remains at 51 % for both days, indicating that the power smoothing methods are effective in maintaining the SC's SOC within the desired range. When applying the EMA and ELES methods, the FSR values for the FC and Elz are significantly reduced to 20 % and 50 % respectively. This reduction indicates that the power smoothing methods successfully suppress power fluctuations, resulting in more stable and controlled operation of the FC and Elz.

Furthermore, Table 5 presents a comprehensive analysis of various scenarios, considering the capacity of the renewable energy sources (PV and HKT), and their impact on the FSR and MSOC indices. Notably, the results demonstrate the crucial role of renewable energy capacity in influencing these performance metrics within the HRES. When evaluating the effect of increasing the capacity of the renewable energy sources, particularly HKT, on the MSOC index, we observe that higher HKT capacity leads to elevated MSOC values. This outcome can be attributed to the non-dispatchable nature of HKT as a renewable energy source. As HKT typically exhibits minimal fluctuations in power output,

Table 4
Fluctuation suppression rate with respect to sources capacity PV/HKT/FC/SC.

System	Day 1			Day 2		
	MSOC (%)	FSR (%)		MSOC (%)	FSR (%)	
		FC	Elz		FC	Elz
PV/HKT/FC/SC	53.75	4.02	82.89	49.23	34.75	10.72
PV/HKT/FC/SC-EMA	53.96	2.89	35.55	49.56	14.88	6.85
PV/HKT/FC/SC-ELES	53.92	2.95	33.40	49.49	14.80	5.78

Table 5
Fluctuation suppression rate with respect to sources capacity.

Capacity (kW)			Day 1			Day 2		
			MSOC (%)	FSR (%)		MSOC (%)	FSR (%)	
PV	HKT	FC		FC	Elz		FC	Elz
20	20	10	53.75	5.96	36.34	49.76	49.20	6.66
20	40	10	53.90	4.03	15.39	49.63	34.77	10.74
30	30	10	53.83	6.67	33.73	49.69	88.59	8.31
30	40	10	53.89	4.00	83.42	49.67	34.71	10.75
40	20	10	53.72	16.71	83.89	49.79	48.90	6.16
40	30	10	53.86	6.65	33.69	49.74	88.78	8.28
40	40	10	53.89	4.02	82.89	49.75	34.75	10.72
40	40	5	53.91	14.01	82.99	49.78	34.51	10.69

the control system can effectively maintain the SC at SOC levels, ensuring its readiness to provide a continuous and stable energy supply.

Similarly, the FSR is significantly impacted by changes in the capacity of the renewable energy sources. In particular, increasing the capacity of HKT results in a notable decrease of up to 4 % in the power fluctuations of the FC. The HKT's ability to smoothen power output reduces the variability experienced by the FC, contributing to a more stable and efficient operation. However, it is important to note that surplus electricity from other renewable sources generates additional fluctuations, which are subsequently stored as H_2 by the Elz. Consequently, the FSR in the output power of Elz is higher due to the intermittent nature of these sources. Nevertheless, with the increase in HKT capacity, the FSR in Elz output power diminishes by up to 20 %, showcasing the benefits of HKT in managing these fluctuations. The behaviour of PV capacity mirrors that of HKT. Adequately increasing the PV capacity ensures a consistent power supply, effectively mitigating significant fluctuations in PV power output. However, the enhanced PV capacity also implies that surplus electricity will experience a higher FSR, leading to its storage as H_2 by Elz.

In summary, Table 5 elucidates the significance of considering renewable energy capacity in optimizing the performance of the HRES. The results underscore the advantages of increasing HKT capacity, which positively influences the MSOC index, and highlights how HKT's power smoothing capabilities contribute to reducing FC fluctuations. By emphasizing the importance of renewable energy capacity, this study provides valuable insights into maximizing the efficiency and reliability of the HRES, ultimately facilitating the integration of RES and promoting sustainable and stable power supply.

5. Conclusions

In conclusion, this paper proposed a novel power smoothing method aimed at reducing PV power fluctuations and enhancing hydrogen production. The method was experimentally validated, and two conventional power smoothing algorithms, EMA and ELES, were compared to generate reference power signals. Through optimization under technical and economic criteria, the system configuration with PV = 40 kW, HKT = 40 kW, FC = 10 kW, Elz = 30 kW, H_2Tank = 30 kg, and SC = 165 F was found to be the optimal solution. The HKT source contributed 46.6 % of the annual electricity demand, resulting in minimal unmet load (0.005 %) and surplus electricity (47.9 %).

The economic analysis revealed a net present cost of USD 210,563 and a levelized cost of 0.19 USD/kWh for the optimal configuration, demonstrating the feasibility of the proposed system. The power smoothing algorithms effectively reduced fluctuations (FSR) by up to 20 % in FC and 50 % in Elz, resulting in a smoother response in hydrogen production. This is a promising outcome, as it enables real-time connection of hydrogen loads in off-grid systems. The proposed energy control mechanism successfully maintained the SC within a high-power smoothing band, allowing the system to respond to PV and demand

fluctuations for longer time intervals.

Moreover, increasing the capacity of HKT proved beneficial as it improved the stability of the HRES, leading to reduced FSR in FC and Elz responses. Lastly, the power signals generated by the EMA algorithm exhibited higher hydrogen consumption compared to ELES, attributed to the averaging characteristic of the method, causing shifts in maximum and minimum power peak values.

In summary, the proposed power smoothing method proved to be effective in reducing power fluctuations, improving hydrogen production, and optimizing the stability and economic performance of the HRES. The combination of RES, PV, HKT, SC, FC, and Elz showcased its potential in providing a reliable and sustainable off-grid electricity supply. By emphasizing the importance of the SC and its role in addressing crucial issues related to PV panels, this research highlights the significance of prioritizing this energy storage component within the HRES. The integration of the SC into the energy control strategy results in an optimized, efficient, and reliable hybrid renewable energy system. Through its capabilities in managing short-term power variations, the SC contributes to improved overall system performance and reliability, ultimately enhancing the integration of renewable energy sources, and facilitating a sustainable and stable power supply. The research highlights the importance of innovative power smoothing strategies for enhancing the integration of RES and hydrogen technologies in off-grid systems.

Declaration of competing interest

The authors declare that they have no known competing financial interests or personal relationships that could have appeared to influence the work reported in this paper.

Data availability

Data will be made available on request.

Acknowledgment

The author (Paul Arévalo) thanks the Call for Grants for the Requalification of the Spanish University System for 2021-2023, Margarita Salas Grants for the training of young doctors awarded by the Ministry of Universities and financed by the European Union –Next Generation EU.

The authors thank Universidad de Cuenca for easing access to the facilities of the Microgrid Laboratory of the Centro Científico Tecnológico y de Investigación Balzay (CCTI-B), for allowing the use of its equipment, and for authorizing its staff the provision of technical support necessary to carry out the experiments described in this paper.

The icons used in this document were developed by www.flaticon.com

The authors acknowledge the support provided by the Thematic Network 723RT0150 “Red para la integración a gran escala de energías renovables en sistemas eléctricos (RIBIERSE-CYTED)” financed by the call for Thematic Networks of the CYTED (Ibero-American Program of Science and Technology for Development) for 2023.

References

[1] K.H. Solangi, M.R. Islam, R. Saidur, N.A. Rahim, H. Fayaz, A review on global solar energy policy, Renew. Sust. Energ. Rev. 15 (2011) 2149–2163, https://doi.org/10.1016/J.RSER.2011.01.007.

[2] A.Q. Al-Shetwi, Sustainable development of renewable energy integrated power sector: trends, environmental impacts, and recent challenges, Sci. Total Environ. 822 (2022), 153645, https://doi.org/10.1016/J.SCITOTENV.2022.153645.

[3] E.E. Gaona, C.L. Trujillo, J.A. Guacaneme, Rural microgrids and its potential application in Colombia, Renew. Sust. Energ. Rev. 51 (2015) 125–137, https://doi.org/10.1016/J.RSER.2015.04.176.

[4] N. Dakota, Solar energy. https://www.ndstudies.gov/energy/level2/module-4-wind-hydropower-solar/solar-power. (Accessed 9 October 2022).

[5] N.A. Ahmed, M. Miyatake, A.K. Al-Othman, Power fluctuations suppression of stand-alone hybrid generation combining solar photovoltaic/wind turbine and fuel cell systems, Energy Convers. Manag. 49 (2008) 2711–2719, https://doi.org/10.1016/J.ENCONMAN.2008.04.005.

[6] A. Ahadi, S.K. Kang, J.H. Lee, A novel approach for optimal combinations of wind, PV, and energy storage system in diesel-free isolated communities, Appl. Energy 170 (2016) 101–115, https://doi.org/10.1016/J.APENERGY.2016.02.110.

[7] A.A. Chen, A.J. Stephens, R. Koon Koon, M. Ashtine, K. Mohammed-Koon Koon, Pathways to climate change mitigation and stable energy by 100% renewable for a small island: Jamaica as an example, Renew. Sust. Energ. Rev. 121 (2020), 109671, https://doi.org/10.1016/J.RSER.2019.109671.

[8] X. Li, D. Hui, X. Lai, Battery energy storage station (BESS)-based smoothing control of photovoltaic (PV) and wind power generation fluctuations, IEEE Trans. Sustain. Energy. 4 (2013) 464–473, https://doi.org/10.1109/TSTE.2013.2247428.

[9] J. Manwell, J.G. Mcgowan, Improvements to the Hybrid2 Battery Model, in: American Wind Energy Association Wind Power, Denver - Colorado, 2005.

[10] G. Wang, M. Ciobotaru, V.G. Agelidis, Power smoothing of large solar PV plant using hybrid energy storage, IEEE Trans. Sustain. Energy. 5 (2014) 834–842, https://doi.org/10.1109/TSTE.2014.2305433.

[11] S. Shivashankar, S. Mekhilef, H. Mokhlis, M. Karimi, Mitigating methods of power fluctuation of photovoltaic (PV) sources - a review, Renew. Sust. Energ. Rev. 59 (2016) 1170–1184, https://doi.org/10.1016/J.RSER.2016.01.059.

[12] L. Valverde, F. Rosa, C. Bordons, J. Guerra, Energy management strategies in hydrogen smart-grids: a laboratory experience, Int. J. Hydrog. Energy 41 (2016) 13715–13725, https://doi.org/10.1016/J.IJHYDENE.2016.05.279.

[13] M.S. Okundamiya, S.T. Wara, H.I. Obakhena, Optimization and techno-economic analysis of a mixed power system for sustainable operation of cellular sites in 5G era, Int. J. Hydrog. Energy 47 (2022) 17351–17366, https://doi.org/10.1016/J.IJHYDENE.2022.03.207.

[14] H. Hassani, F. Zaouche, D. Rekioua, S. Belaid, T. Rekioua, S. Bacha, Feasibility of a standalone photovoltaic/battery system with hydrogen production, J. Energy Storage. 31 (2020), 101644, https://doi.org/10.1016/J.EST.2020.101644.

[15] D.N. Luta, A.K. Raji, Decision-making between a grid extension and a rural renewable off-grid system with hydrogen generation, Int. J. Hydrog. Energy 43 (2018) 9535–9548, https://doi.org/10.1016/J.IJHYDENE.2018.04.032.

[16] M. Temiz, N. Javani, Design and analysis of a combined floating photovoltaic system for electricity and hydrogen production, Int. J. Hydrog. Energy 45 (2020) 3457–3469, https://doi.org/10.1016/J.IJHYDENE.2018.12.226.

[17] D.N. Luta, A.K. Raji, Optimal sizing of hybrid fuel cell-supercapacitor storage system for off-grid renewable applications, Energy. 166 (2019) 530–540, https://doi.org/10.1016/J.ENERGY.2018.10.070.

[18] M.B. Abdelghany, M. Faisal Shehzad, D. Liuzza, V. Mariani, L. Glielmo, Modeling and optimal control of a hydrogen storage system for wind farm output power smoothing, in: Proceedings of the IEEE Conference on Decision and Control, Institute of Electrical and Electronics Engineers Korea (South), 2020, pp. 49–54, https://doi.org/10.1109/CDC42340.2020.9304133.

[19] L. Kong, L. Li, G. Cai, C. Liu, P. Ma, Y. Bian, T. Ma, Techno-economic analysis of hydrogen energy for renewable energy power smoothing, Int. J. Hydrog. Energy 46 (2021) 2847–2861, https://doi.org/10.1016/J.IJHYDENE.2020.07.231.

[20] A. Takahashi, A. Goto, Y. Machida, S. Funabiki, A power smoothing control method for a photovoltaic generation system using a water electrolyzer and its filtering characteristics, Electr. Eng. Jpn. 206 (2019) 25–32, https://doi.org/10.1002/EEJ.23191.

[21] L. Kong, J. Yu, G. Cai, Modeling, control and simulation of a photovoltaic /hydrogen/ supercapacitor hybrid power generation system for grid-connected applications, Int. J. Hydrog. Energy 44 (2019) 25129–25144, https://doi.org/10.1016/J.IJHYDENE.2019.05.097.

[22] P.B. Nempu, J.N. Sabhahit, D.N. Gaonkar, V.S. Rao, Novel power smoothing technique for a hybrid AC-DC microgrid operating with multiple alternative energy sources, Adv. Electr. Comput. Eng. 21 (2021) 99–106, https://doi.org/10.4316/AECE.2021.02011.

[23] S.G. Tesfahunegn, Ulleberg, P.J.S. Vie, T.M. Undeland, Optimal shifting of Photovoltaic and load fluctuations from fuel cell and electrolyzer to lead acid battery in a Photovoltaic/hydrogen standalone power system for improved performance and life time, J. Power Sources 196 (2011) 10401–10414, https://doi.org/10.1016/J.JPOWSOUR.2011.06.037.

[24] A. Takahashi, J. Imai, S. Funabiki, Experimental verification of suppressing power fluctuation in photovoltaic generation system using water electrolyzer, in: INTELEC, International Telecommunications Energy Conference (Proceedings), Institute of Electrical and Electronics Engineers (Broadbeach, QLD, Australia), 2017, pp. 562–565, https://doi.org/10.1109/INTLEC.2017.8214196.

[25] M.R. Barakat, B. Tala-Ighil, H. Gualous, D. Hissel, Modeling of a hybrid marine current-hydrogen active power generation system, Int. J. Hydrog. Energy 44 (2019) 9621–9635, https://doi.org/10.1016/J.IJHYDENE.2018.10.020.

[26] Hydrologic Engineering Center's (CEIWR-HEC), River Analysis System (HEC-RAS) website. https://www.hec.usace.army.mil/software/hec-ras/. (Accessed 9 October 2022).

[27] Meteorological information of rivers in Ecuador, National Institute of Meteorology and Hydrology (INAMHI). https://https://www.inamhi.gob.ec/. (Accessed 9 October 2022).

[28] A. Cano, P. Arévalo, D. Benavides, F. Jurado, Comparative analysis of HESS (battery/supercapacitor) for power smoothing of PV/HKT, simulation and experimental analysis, J. Power Sources 549 (2022), 232137, https://doi.org/10.1016/J.JPOWSOUR.2022.232137.

[29] Information on Public Investment in Ecuador, National Secretariat of Planning. https://www.planificacion.gob.ec/informacion-de-inversion-publica/. (Accessed 13 August 2022).

[30] Inflation Report in the Ecuadorian sector, Ecuadorian Central Bank. https://www.bce.fin.ec/index.php/component/k2/item/317-informe-de-inflacion. (Accessed 13 August 2022).
[31] J.L. Espinoza, L.G. Gonzalez, R. Sempertegui, Micro grid laboratory as a tool for research on non-conventional energy sources in Ecuador, in: 2017 IEEE International Autumn Meeting on Power, Electronics and Computing, ROPEC 2017, Institute of Electrical and Electronics Engineers (Ixtapa, Mexico), 2018, pp. 1–7, https://doi.org/10.1109/ROPEC.2017.8261615.
[32] K. Mongird, V. Viswanathan, J. Alam, C. Vartanian, V. Sprenkle, R. Baxter, Grid Energy Storage Technology Cost and Performance Assessment, 2020, 2020.
[33] P. Arévalo, F. Jurado, Performance analysis of a PV/HKT/WT/DG hybrid autonomous grid, Electr. Eng. 103 (2021) 227–244, https://doi.org/10.1007/S00202-020-01065-9/TABLES/3.
[34] X. Zhang, Q.S. Wei, B.S. Oh, Cost analysis of off-grid renewable hybrid power generation system on Ui Island, South Korea, Int. J. Hydrog. Energy 47 (2022) 13199–13212, https://doi.org/10.1016/J.IJHYDENE.2022.01.150.
[35] P. Arévalo, A. Cano, F. Jurado, Comparative study of two new energy control systems based on PEMFC for a hybrid tramway in Ecuador, Int. J. Hydrog. Energy 45 (2020) 25357–25377, https://doi.org/10.1016/J.IJHYDENE.2020.06.212.
[36] M. Belouda, M. Hajjaji, H. Sliti, A. Mami, Bi-objective optimization of a standalone hybrid PV–wind–battery system generation in a remote area in Tunisia, Sustain. Energy Grids Netw. 16 (2018) 315–326, https://doi.org/10.1016/J.SEGAN.2018.09.005.
[37] L.G. González, R. Chacon, B. Delgado, D. Benavides, J. Espinoza, Study of energy compensation techniques in photovoltaic solar systems with the use of supercapacitors in low-voltage networks, Energies 13 (2020) 3755, https://doi.org/10.3390/EN13153755.
[38] P.M. Diéguez, A. Ursúa, P. Sanchis, C. Sopena, E. Guelbenzu, L.M. Gandía, Thermal performance of a commercial alkaline water electrolyzer: experimental study and mathematical modeling, Int. J. Hydrog. Energy 33 (2008) 7338–7354, https://doi.org/10.1016/J.IJHYDENE.2008.09.051.
[39] X. Shen, X. Zhang, G. Li, T.T. Lie, L. Hong, Experimental study on the external electrical thermal and dynamic power characteristics of alkaline water electrolyzer, Int. J. Energy Res. 42 (2018) 3244–3257, https://doi.org/10.1002/ER.4076.
[40] J. Jia, Q. Li, Y. Wang, Y.T. Cham, M. Han, Modeling and dynamic characteristic simulation of a proton exchange membrane fuel cell, IEEE Trans. Energy Convers. 24 (2009) 283–291, https://doi.org/10.1109/TEC.2008.2011837.
[41] A. Fathy, H. Rezk, Multi-verse optimizer for identifying the optimal parameters of PEMFC model, Energy. 143 (2018) 634–644, https://doi.org/10.1016/J.ENERGY.2017.11.014.
[42] Y.J. Sohn, S.D. Yim, G.G. Park, M. Kim, S.W. Cha, K. Kim, PEMFC modeling based on characterization of effective diffusivity in simulated cathode catalyst layer, Int. J. Hydrog. Energy 42 (2017) 13226–13233, https://doi.org/10.1016/J.IJHYDENE.2017.04.036.
[43] J.G. Silva, J.O. De Aquino Limaverde, E.L. Feitosa Filho, Fortaleza., Adaptive extended Kalman filter using exponencial moving average, IFAC 51 (2018) 208–211, https://doi.org/10.1016/J.IFACOL.2018.11.106.
[44] K.A. Naik, C.P. Gupta, Output power smoothing and voltage regulation of a fixed speed wind generator in the partial load region using STATCOM and a pitch angle controller, Energies 11 (2018) 58, 11 (2017) 58, https://doi.org/10.3390/EN11010058.
[45] E. Usaratniwart, S. Sirisukprasert, N. Hatti, M. Hagiwara, A case study in micro grid using adaptive enhanced linear exponential smoothing technique, in: 2017 8th International Conference on Information and Communication Technology for Embedded Systems, (Chonburi, Thailand), 2017, https://doi.org/10.1109/ICTEMSYS.2017.7958776.
[46] HOMER, Pro - microgrid software for designing optimized hybrid microgrids. https://www.homerenergy.com/products/pro/index.html. (Accessed 11 October 2022).
[47] P. Arévalo, D. Benavides, J. Lata-García, F. Jurado, Energy control and size optimization of a hybrid system (photovoltaic-hidrokinetic) using various storage technologies, Sustain. Cities Soc. 52 (2020), 101773, https://doi.org/10.1016/j.scs.2019.101773.